RSC Advances

PAPER

View Article Online
View Journal | View Issue

Open Access Article. Published on 17 June 2025. Downloaded on 11/7/2025 8:09:35 PM.
This article is licensed under a Creative Commons Attribution-NonCommercial 3.0 Unported Licence.

Check for updates

Cite this: *RSC Adv.*, 2025, **15**, 17186

Phenyltriazole-based sulfonamides: novel dual-target agents against MRSA biofilms and resistant pathogens†

Abdelrahman Hussien,[a] Arafa Musa,*[b] Hanzada T. Nour El-Din,[c] Ahmed M. Helal,[a] Yosra I. Nagy,[c] Hany G. Ezzat,[a] Ahmed S. Attia,[cd] Abdelrahman S. Mayhoub,[ae] Khaled Shalaby,[f] Della Grace Thomas Parambi[g] and Mohamed M. Elsebaie *[a]

The advent of multidrug-resistant bacteria requires the continuous development of new antimicrobial agents. A series of phenyltriazole–sulfonamide hybrid compounds (**16–27**) have been synthesized and evaluated for their antimicrobial properties, with a focus on combating resistant bacterial strains such as methicillin-resistant *Staphylococcus aureus* (MRSA) and *Acinetobacter baumannii* AB5075. Compounds were synthesized through a multi-step reaction, including alkylation and aminoguanidine substitution, with structural elucidation performed using NMR and elemental analysis. Antimicrobial activity was assessed through Minimum Inhibitory Concentration (MIC) measurements, which revealed that compounds with longer alkyl chains or specific functional groups had a very enhanced activity against MRSA, especially **23** and **24** analogs. The results highlighted the correlation between lipophilicity (log *P*) and antimicrobial efficacy, particularly for compounds such as **23** (*n*-nonyl) which showed potent activity against MRSA. Further evaluation by time-killing assays demonstrated the rapid bactericidal activity of compound **23**, while biofilm disruption studies showed the potential of these compounds to target biofilm-associated infections. Docking studies have shown that these compounds can interact with key bacterial targets, including PBP2a and DHPS, providing a dual-target approach for treatment of MRSA. Furthermore, *in silico* analysis revealed favorable pharmacokinetic and ADME properties of the synthesized compounds. The study shows promising new candidates for combating antimicrobial resistance, with the potential for further optimization and development.

Received 7th April 2025
Accepted 12th May 2025

DOI: 10.1039/d5ra02412a

rsc.li/rsc-advances

1. Introduction

Methicillin-resistant *Staphylococcus aureus* (MRSA) poses a significant global health threat due to its resistance to multiple antibiotics, leading to high morbidity and mortality in nosocomial and community-acquired infections.[1] The emergence of vancomycin-resistant strains and biofilm-associated infections further complicates treatment, necessitating the development of novel antimicrobial agents. Sulfonamide-based compounds, historically effective against bacterial infections, offer a promising scaffold for designing new anti-MRSA agents. This study evaluates the antimicrobial activity of phenyltriazole–sulfonamides, a novel class of compounds combining triazole and sulfonamide moieties, against MRSA, with a focus on their anti-biofilm properties, time-kill kinetics, and computational ADME profiles.[2,3] Studies on the different bacterial targets of existing antibiotics have revealed that antibiotics do not target all the major biochemical pathways in bacteria. Fortunately, most antibiotics work by selectively inhibiting specific bacterial processes, such as cell wall synthesis (peptidoglycan),[4,5] protein synthesis (translation),[6,7] DNA replication,[8,9] RNA synthesis (transcription),[10] and folic acid biosynthesis.[11] Only a small number of antibiotics act by interfering with ion channels or promoting bacterial cell lysis.[12–14]

According to a report by the World Health Organization (WHO), there is a global shortage of effective antibacterial agents for both Gram-negative and Gram-positive bacteria.[15]

[a]Department of Pharmaceutical Organic Chemistry, College of Pharmacy, Al-Azhar University, Cairo 11884, Egypt. E-mail: m.elsebaei@azhar.edu.eg

[b]Department of Pharmacognosy, College of Pharmacy, Jouf University, Sakaka, Aljouf 72341, Saudi Arabia. E-mail: akmusa@ju.edu.sa

[c]Department of Microbiology and Immunology, Faculty of Pharmacy, Cairo University, Cairo, 11562, Egypt

[d]Department of Microbiology and Immunology, School of Pharmacy, Newgiza University, Giza, Egypt

[e]Biomedical Sciences, University of Science and Technology, Zewail City of Science and Technology, Giza, Egypt

[f]Department of Pharmaceutics, College of Pharmacy, Jouf University, Sakaka, Aljouf 72341, Saudi Arabia

[g]Department of Pharmaceutical Chemistry, College of Pharmacy, Jouf University, Sakaka, Aljouf 72341, Saudi Arabia

† Electronic supplementary information (ESI) available. See DOI: https://doi.org/10.1039/d5ra02412a

© 2025 The Author(s). Published by the Royal Society of Chemistry

Open Access Article. Published on 17 June 2025. Downloaded on 11/7/2025 8:09:35 PM.
This article is licensed under a Creative Commons Attribution-NonCommercial 3.0 Unported Licence.

Despite extensive efforts, the main reason for the persistence of bacterial infections is the development of resistance.[16] Therefore, the current need to advance the development of novel antibacterial categories. The emergence of multidrug-resistant microorganisms is one of the most urgent global challenges.[17] Examples of bacterial infections that have developed resistance to multiple drugs are *Streptococcus pneumoniae*, methicillin-resistant *Staphylococcus aureus* (MRSA), *Pseudomonas aeruginosa*, *Acinetobacter baumannii*, *Escherichia coli*, vancomycin-resistant enterococci (VRE), and *Klebsiella pneumoniae*.

Among these, *Staphylococcus aureus* is notable for its versatility. It can colonize the skin and other body parts, even without symptoms of active disease, and about 20% of the world's population are thought to be carriers of the pathogen. Normally, it remains inactive until the skin breaks or the immune system weakens, allowing the bacteria to enter the body and cause infection. This results in the appearance of diseases caused by toxins produced by the bacteria themselves, and rapid proliferation of the organism, resulting in invasion and destruction of tissues.[18] The reason for our particular interest in this pathogen is the lack of comprehensive data on the distribution of MRSA clones in the Middle East, particularly in Egypt.[19]

Infections with *S. aureus* are usually self-limiting and not immediately life-threatening, but there is a growing concern that these infections are increasingly penetrating deeper into the tissues, and leading to more serious and potentially life-threatening diseases. The main problem is that *S. aureus* has developed resistance to the most effective antibacterial agents previously available. To address this problem, it is necessary to develop new drugs that can effectively combat this adaptable microorganism, which is very versatile.[20] As *S. aureus* can occur naturally in human skin and in the nasal cavity, it is often associated with infections of the skin and soft tissue. However, microorganisms can spread from superficial locations to deeper and more critical areas. This dissemination may occur *via* the bloodstream, allowing *S. aureus* to establish metastatic foci of infection in distant locations.[21] Diseases caused by *S. aureus* can be attributed to the broad spectrum of cell surface and extracellular protein toxins produced by the bacterium which actively antagonize the host defences. In addition, *S. aureus* may express several surface-localized proteins that bind to components of the extracellular matrix and serve as adhesins that facilitate bacterial binding and colonization. The cytolytic toxins produced by *S. aureus* may damage the membranes of host cells, while superantigens may cause toxic shock syndrome.[22]

Another example of a resistant bacterial infection is *Acinetobacter baumannii*, a Gram-negative bacterium. Gram-negative bacteria have an impermeable outer membrane that prevents many chemical compounds from entering. This makes porin channels a prime entry point for antibacterial agents.[23] These porins are lined with highly charged residues such as arginine, aspartate, and glutamate.[24] The physicochemical properties of antibacterial compounds are therefore crucial for researchers. In general, compounds that target Gram-negative bacteria must have a higher degree of polarity than compounds that have limited activity against Gram-negative strains.[25]

The sulfonamide moiety is present in many medications. Examples include the antibiotics sulfamethoxazole (also known as cotrimoxazole when combined with trimethoprim), chlorthalidone, a thiazide-like diuretic, zonisamide, a drug used to treat treatment of epilepsy and Parkinson's disease, and acetazolamide, carbonic anhydrase inhibitors, and dorzolamide used to treat high blood pressure in the eye, also with glaucoma, and many more,[26] (Fig. 1).

In our laboratory, our focus in recent years has been the synthesis of various antibacterial agents with potent activity against a broad spectrum of both Gram-negative and Gram-positive bacteria. This work was mainly based on the identification of our lead compound phenylthiazole, which had a lipophilic part and a polar part of the guanidine moiety. However, its activity was mainly observed against Gram-positive pathogens.[27] Several structural optimization processes have been performed to improve antimicrobial activity and metabolic stability.[28–42] Despite phenylthiazole's remarkable success in eliminating intracellular pathogens and reducing the bacterial biofilm burden, rapid and lethal mode of action, its activity against Gram-negative microorganisms was significantly limited and limited only to Gram-positive pathogens. However, their low activity against Gram-negative pathogens has been mainly attributed to their poor permeability to Gram-negative

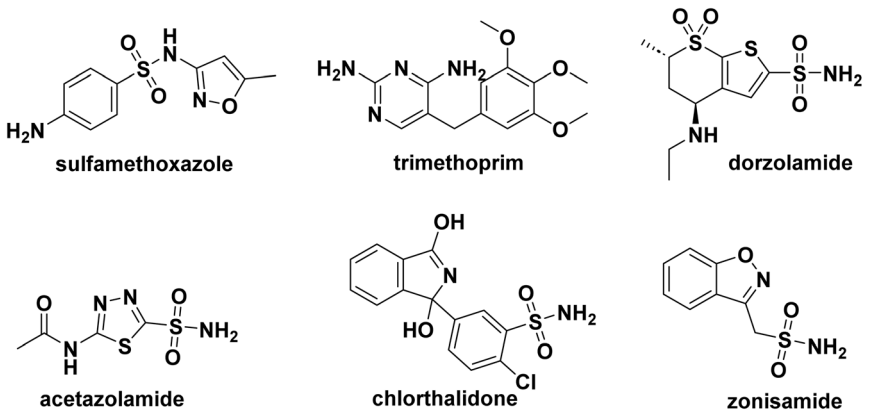

Fig. 1 The structure of approved sulfonamide drugs.

Open Access Article. Published on 17 June 2025. Downloaded on 11/7/2025 8:09:35 PM.
This article is licensed under a Creative Commons Attribution-NonCommercial 3.0 Unported Licence.

pathogens, as recent studies have confirmed that phenylthiazoles exert their action by inhibiting the two major proteins involved in the synthesis of undecaprenylpyrophosphate phosphatase (UppP) and undecaprenylpyrophosphate synthase (UppS) in the cell wall. Consequently, when the phenylthiazole core was replaced by phenylpyrazoles, a significant improvement in polarity and activity against Gram-negative bacteria was observed.[34,43–45] As manifested in the rationalization of work (Fig. 2), introducing a polarized pharmacophore to the phenyltriazole scaffold enhances its' antimicrobial activity and pharmacokinetic properties.

Taken together, phenyltriazole–sulfonamide conjugates offer a strong potential for dual interaction on MRSA targets. The chemical moieties within the novel design include phenyltriazole moiety with terminal polar guanidine to prove their ability to cross the cell wall of MRSA and cause disruption.[5] Thus, the incorporation of active sulfonamide pharmacophore may potentiate the antimicrobial activity by inhibiting the folate pathway. Moreover, this design would have a higher polarity and therefore higher activity with a wider spectrum of antibacterial effectiveness. Several structural modifications have been made to improve both antibacterial activities, including

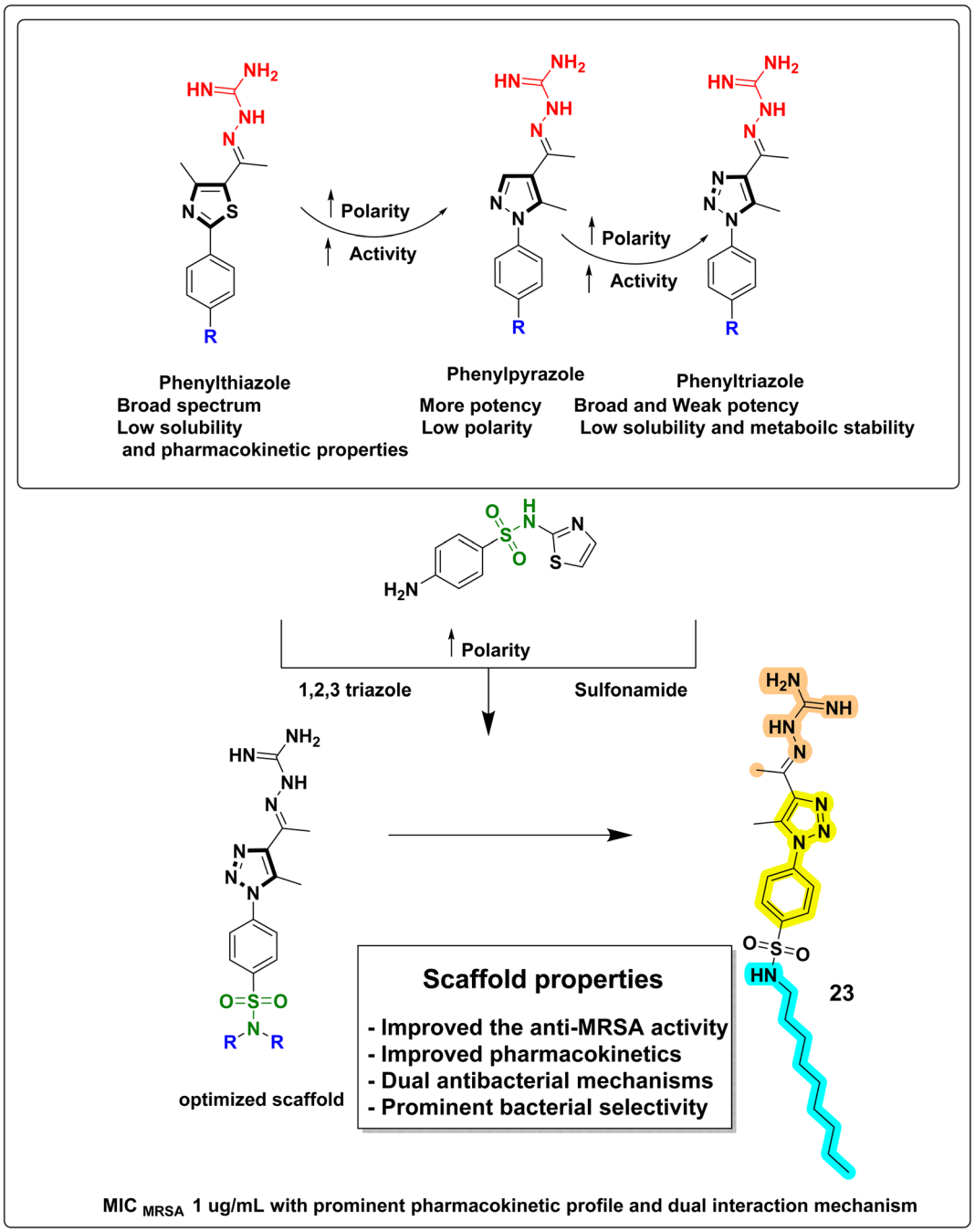

Fig. 2 Rational design of phenyltriazole–sulfonamides hybrids.

 © 2025 The Author(s). Published by the Royal Society of Chemistry

Open Access Article. Published on 17 June 2025. Downloaded on 11/7/2025 8:09:35 PM.
This article is licensed under a Creative Commons Attribution-NonCommercial 3.0 Unported Licence.

anti-biofilm activity and intracellular pathogen control, and to improve the pharmacokinetic profile. However, the solubility of the resulting compounds proved to be somewhat unsatisfactory. One of the key factors in increasing the solubility of these compounds was the linker between the head and the scaffold.[46–48] A new class of phenyltriazoles was therefore synthesized and evaluated for antibacterial activity. Phenyltriazoles included in this study have been designed to contain a sulfonamide moiety (Fig. 2), which is known to have antibacterial activity.[49]

2. Results and discussion

2.1 Chemistry

Our compounds **1–27** have been synthesised as described in (Fig. 3). The resulting structures of compounds **3–27** was elucidated by means of spectrum data and elemental analysis, as shown in the ESI.† Sulphanilamide was dissolved in 6 M HCl, and equal amount of THF and DMF, then cooled to 0 °C in an ice-bath and $NaNO_2$ was dissolved in H_2O and added dropwise to the solution and the reaction was stirred for 25 minutes. NaN_3 was dissolved in H_2O and then added dropwise with stirring and allowed to gradually warm to room temperature overnight. The reaction mixture is poured into H_2O, then extracted three times with ethyl acetate. The combined organic layer was washed with saturated bicarbonate solution and brine solution. The organic layer was then dried over anhydrous sodium sulfate and evaporated under reduced pressure and used in the second step as a yellow solid without further purification.[49]

Compound **2** was dissolved in ethanol. Acetylacetone and sodium ethoxide were added. The reaction was heated to reflux stirring for 4–6 hours. After the reaction was completed and allowed to cool to room temperature, the white solid was precipitated and then filtered to give compound **3**. Compound **3** was dissolved in DMF, K_2CO_3 and appropriate alkyl halides were added. The reaction was then stirred at 75 °C for 1 hour. The reaction was monitored with TLC until the starting material disappeared. The reaction mixture was allowed to cool and poured into ice-cold water to afford compounds **4–15** as a white solid.

The alkylated triazole acetyl compounds **4–15** were dissolved in ethanol, 1 ml conc. hydrochloric acid and aminoguanidine bicarbonate were added. The reaction mixture was refluxed for 6 hours, after completion of the reaction, it was poured into ice-cold water and neutralized with sodium carbonate to afford compounds **16–27**. The chemical structure of compounds **16–27** was confirmed based on their spectral data and elemental analysis. In addition to the signals corresponding to the phenyltriazole scaffold and its two methyl groups, which appeared in all ^{1}H NMR and ^{13}C NMR spectra at almost the same chemical shifts at around 2.55–2.3 ppm, the ^{1}H NMR spectrum

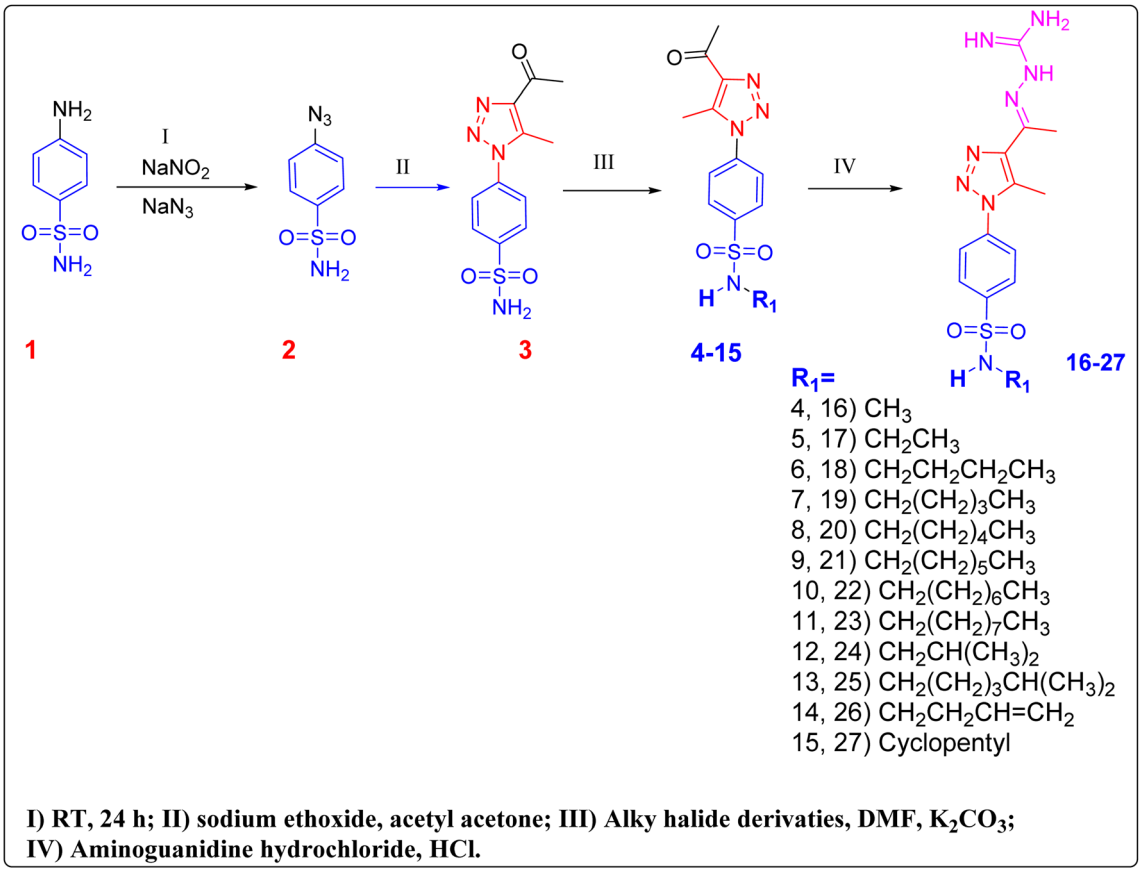

Fig. 3 Synthesis of phenyltriazole–sulfonamides hybrids.

Open Access Article. Published on 17 June 2025. Downloaded on 11/7/2025 8:09:35 PM.
This article is licensed under a Creative Commons Attribution-NonCommercial 3.0 Unported Licence.

of compounds **11** and **23**, as examples, exhibited additional multiplet signals at 1.42–0.85 ppm, in the aliphatic region due to the presence of the nonyl aliphatic moiety and the whole aliphatic chain appeared in ^{13}C NMR spectrum as 9 signals from δ 43.04 to 15.95. Also, for the rest of the compound's NMR spectra showed obvious signals at the aliphatic region which indicates the addition of the different alkyl halides to the starting compound.

Subsequently, the reaction of **4–15** with aminoguanidine hydrochloride gave the final products **16–27** as outlined in Fig. 3. The structures of this series of novel compounds were confirmed by their spectral and elemental data. The guanidyl protons, for **24** as a representative example, displayed in the ^{1}H NMR spectrum as broad signals at δ 5.68 ppm and these signals showed approximately the same ppm for each compound to ensure the formation of the intended aminoguanidine products.

2.2 Biological evaluation

2.2.1 Antimicrobial assessment and SAR study. Antimicrobial resistance represents is a major public health concern and requires further evaluation of new compounds for their effectiveness against resistant bacterial strains. In this context, the antimicrobial evaluation of synthesized compounds is crucial to identify potential therapeutic agents. This study focused on compounds **16–27**, that have been systematically evaluated for their antimicrobial activity against methicillin-resistant *Staphylococcus aureus* (MRSA) and *Acinetobacter baumannii* AB5075; two clinically relevant pathogens known for their resistance to conventional antibiotics. To determine the potency of these compounds, the minimum inhibitory concentrations (MICs) were measured by investigating the antimicrobial properties of these compounds, this study aims to contribute to the development of new treatments that can effectively combat resistant bacterial infections. The data provided in Table 1 and Fig. 4 presents the minimum inhibitory concentrations (MIC) of a series of substituted sulphamoyl 1,2,3-phenyl triazoles against two clinically relevant multidrug-resistant bacterial strains, methicillin-resistant *Staphylococcus aureus* (*S. aureus* USA300) and *Acinetobacter baumannii* AB5075. Additionally, the table provides the lipophilicity (log *P*) values for the compounds, offering a basis for understanding the relationship between the chemical structure of the derivatives and their antimicrobial activity. A comprehensive Structure–Activity Relationship (SAR) analysis allows us to identify key structural features that influence the antimicrobial potency against these bacterial strains. The compounds tested in this study feature variations in alkyl chain length and branching, as well as the presence of specific functional groups. These variations result in substantial changes in antimicrobial efficacy, which can be explained by their effect on physicochemical properties, such as lipophilicity, and their ability to interact with bacterial targets. A clear trend emerges when examining the effect of alkyl chain length on antimicrobial activity. Shorter alkyl groups (methyl, ethyl, *n*-butyl, *n*-pentyl, and *n*-hexyl) generally show poor to moderate activity against both *S. aureus* and *A. baumannii*, with MIC values greater than 64 μg ml^{-1} for most of these compounds. Notably, compounds with shorter chains (**16–20**) exhibit significantly reduced activity against both bacterial strains, highlighting the importance of hydrophobicity and the optimal size of the alkyl group in penetrating bacterial membranes and affecting their target sites.

Table 1 Susceptibility data for target compounds and control drug *vs.* methicillin-resistant *Staphylococcus aureus* and *Acinetobacter baumannii* AB5075 as minimum inhibitory concentration (MIC in μg ml^{-1}) values[a]

Cp. ID	R	*S. aureus* USA300	*A. baumannii* AB5075	Log *P* value
16	Methyl	>64	>64	0.62
17	Ethyl	>64	>64	1.15
18	*n*-Butyl	>64	>64	2.20
19	*n*-Pentyl	>64	>64	2.73
20	*n*-Hexyl	16	16	3.26
21	*n*-Heptyl	64	>64	3.79
22	*n*-Octyl	64	64	4.32
23	*n*-Nonyl	1	64	4.85
24	Isobutyl	4	8	2.07
25	Heptan-2-yl	>64	>64	3.57
26	But-3-en-1-yl	>64	>64	1.72
27	Cyclopentyl	8	32	2.09
Vancomycin	—	1	NT	−1.14

[a] NT: not tested.

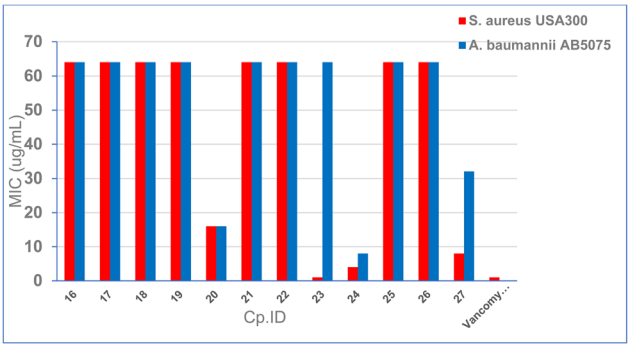

Fig. 4 Bar chart showing the antimicrobial data of phenyltriazole–sulfonamide hybrids.

However, the introduction of longer alkyl chains appears to improve antimicrobial efficacy against *S. aureus* but not necessarily against *A. baumannii*. For instance, compound **23** (*n*-nonyl) exhibits a marked reduction in MIC against *S. aureus* (1 μg ml^{-1}), but maintains a higher MIC against *A. baumannii* (64 μg ml^{-1}). This suggests that while increased lipophilicity (as indicated by a higher log *P* value of 4.85) may enhance membrane penetration and bactericidal activity against *S. aureus*, it does not guarantee activity against *A. baumannii*, which may have different membrane properties or efflux mechanisms that limit the effectiveness of these compounds.

Additionally, cyclopentyl analog **27** and branched alkyl groups (**24**, Isobutyl) also demonstrate notable activity. Cyclopentyl (MIC = 8 μg ml^{-1} for *S. aureus* and 32 μg ml^{-1} for *A.*

 © 2025 The Author(s). Published by the Royal Society of Chemistry

Open Access Article. Published on 17 June 2025. Downloaded on 11/7/2025 8:09:35 PM.
This article is licensed under a Creative Commons Attribution-NonCommercial 3.0 Unported Licence.

baumannii) and isobutyl (MIC = 4 μg ml^{-1} for *S. aureus* and 8 μg ml^{-1} for *A. baumannii*) derivatives show moderate to good antimicrobial activity, suggesting that such substitutions might provide steric or electronic benefits that enhance bacterial cell interaction, potentially *via* changes in the binding or affinity to bacterial targets. These branched and cyclic groups may also hinder bacterial efflux mechanisms, contributing to their improved activity. A noteworthy observation is the correlation between lipophilicity (log *P*) and antimicrobial activity. As the alkyl chain length increases, the log *P* value also increases, suggesting an enhanced ability of these compounds to partition into the lipid bilayer of bacterial membranes. For example, compound **16** (methyl group, log *P* = 0.62) exhibits no antimicrobial activity, whereas compound **23** (*n*-nonyl, log *P* = 4.85) demonstrates significant activity against *S. aureus* (MIC = 1 μg ml^{-1}). However, the correlation between log *P* and MIC is not straightforward, as shown by compound **21** (*n*-heptyl, log *P* = 3.79) which has high MIC values (64 μg ml^{-1}) against both bacterial strains. This suggests that while log *P* is a contributing factor to antimicrobial activity, other structural features, such as the nature of the alkyl group, might play a more dominant role in determining activity. It also indicates that the compounds in this study, while effective against *S. aureus*, may not be as effective against *A. baumannii* unless further structural modifications are made to address specific resistance mechanisms in *A. baumannii*.

2.2.2 Time-killing assay. Methicillin-resistant *Staphylococcus aureus* (MRSA) remains among the most challenging bacterial pathogens. It is responsible for several difficult-to-treat infections due to its resistance to commonly used antibiotics, including methicillin and other beta-lactams. This growing resistance has led to an urgent need for new antimicrobial agents to effectively combat MRSA infections. In this context, vancomycin, a glycopeptide antibiotic, has been a mainstay in the treatment of MRSA; however, increasing resistance and sometimes limited effectiveness have driven the search for alternative therapies. To address this issue, two novel compounds **23** and **24**, were evaluated for their antibacterial activity (Fig. 5) compared to vancomycin against methicillin-resistant *Staphylococcus aureus* (MRSA) over 24 hours. The *y*-axis represents the logarithm of colony-forming units per milliliter (CFU ml^{-1}) of MRSA and indicates bacterial concentration, while the *x*-axis shows time in hours. Phenyltriazole with linear side chains (nonyl **23**) exhibited rapid bactericidal activity against MRSA and complete eradication from about 6 CFU ml^{-1} to nearly 0.09 CFU ml^{-1} within 8 hours, indicating potent antibacterial activity. On the other hand, compound **24**, like vancomycin, shows a decrease in MRSA counts, but is slightly less effective than compound **23**, reaching about 1.50 CFU ml^{-1} after 24 hours. These results suggest that both compounds could be viable alternatives to vancomycin, particularly compound **23**, which shows faster and more effective MRSA suppression.

2.2.3 Anti-biofilm effect. A crucial factor in the development of new antibiotics is their ability to inhibit bacterial virulence mechanisms, particularly biofilm formation. Biofilms are structured bacterial communities surrounded by a self-produced protective matrix, that provides defense against antibiotics and the host's immune system. This protective barrier often leads to chronic and persistent infections, especially in clinical settings where biofilms often form on medical devices. The resilience of biofilms makes the treatment of biofilm-associated infections a significant challenge.

To address this issue, the development of antibacterial agents with potent anti-biofilm activity is essential. Compounds **23** and **24** were investigated for their ability to eradicate preformed, mature biofilms of methicillin-resistant *Staphylococcus aureus* (MRSA), Fig. 6. The green bars show that compound **23** achieves a high percentage of biofilm disruption, with around 70–80% indicating it is effective in disrupting MRSA biofilms, which are known to protect bacteria from antibiotic effects. While compound **24**, the blue bars show that compound **24** also disrupts biofilm, although to a slightly lesser extent than compound **23**, with disruption percentages typically lower than compound **23**. These results suggest that these compounds are promising alternatives or complements. These compounds may offer advantages over current MRSA treatments especially in treating infections associated with biofilms where traditional antibiotics are less effective.

2.3 *In silico* studies

2.3.1 Docking and binding affinity analyses of 23 analog. Methicillin-resistant *Staphylococcus aureus* (MRSA) is a major clinical concern due to its resistance to a broad spectrum of β-

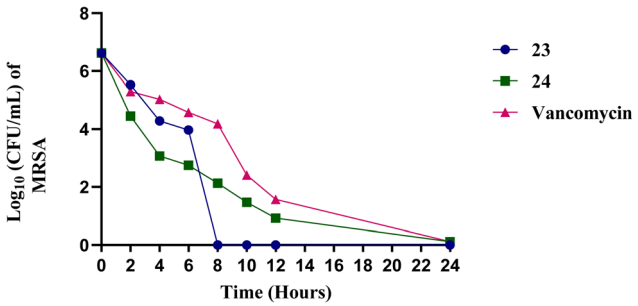

Fig. 5 Time-kill analysis of compounds against MRSA. Compounds **31**, **32** and vancomycin (4× MIC) against MRSA USA300 over a 24-hour incubation period at 37 °C.

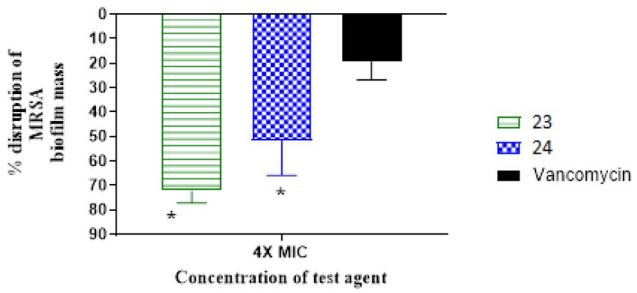

Fig. 6 Disruption of mature MRSA USA300 biofilms by phenyltriazole compounds and ceftriaxone (at 4× MIC). Data are shown as the percentage of biofilm disruption relative to untreated controls.

Open Access Article. Published on 17 June 2025. Downloaded on 11/7/2025 8:09:35 PM.
This article is licensed under a Creative Commons Attribution-NonCommercial 3.0 Unported Licence.

lactam antibiotics, primarily mediated by the penicillin-binding protein 2a (PBP2a).[50–52] In addition to PBP2a, *S. aureus* also relies on the dihydropteroate synthase (DHPS) enzyme for folic acid biosynthesis, a key pathway for bacterial survival. The development of dual-targeted therapies that inhibit both PBP2a and DHPS represents a promising strategy to combat MRSA infections, especially as the emergence of antibiotic resistance continues to threaten the effectiveness of current treatments.[13,53] Phenyltriazole–sulfonamide conjugates have emerged as potential candidates for such dual inhibition, offering a new class of compounds with enhanced antibacterial activity against MRSA. Phenyltriazole–sulfonamide conjugates are designed by linking phenyltriazole groups, which are known to interact with bacterial enzymes, to sulfonamide moieties that target the DHPS enzyme. The phenyltriazole group has been shown to have antimicrobial activity by disrupting bacterial cell wall synthesis, while the sulfonamide moiety interferes with folic acid biosynthesis. By targeting two essential enzymes, PBP2a and DHPS, these conjugates hold the potential to bypass some of the resistance mechanisms that MRSA employs to evade treatment.[54]

Therefore, the binding affinity of potent analogs based on the inhibitory effect on MRSA and other microbial strains to both targets was therefore examined using inhibition constant data; K_i is an effective parameter for cell wall destruction and inhibition of folate biosynthesis. The docking score of potent analogs **23** and **24** are estimated and the inhibitor constant, K_i, is calculated using the equation (Table 2). The equation used for K_i calculation is as follows:

$$K_i = \exp(\Delta G/(R \times T)), (T = 298\ \mathrm{K})$$

Data revealed potent inhibitory data activity of both compounds on both target cell walls and DNA synthesis pathways; 34–26 nM consistent with antimicrobial activity against target strains which enforce the targets probability. The presence of such structural pharmacophores as triazole, sulfonamid, and guanidine base predispose it to be the same mechanism. The Polar Surface Area (PSA), an important descriptor of molecular polarity, is often associated with key pharmacokinetic properties such as bioavailability, solubility, and membrane permeability. Both compounds showed uniform PSA that assist in the enzyme interactions and antimicrobial activity reflecting molecular size and polarity. The results show that both compounds have hemolytic concentrations (LC) of more than 10 mg ml^{-1}, indicating minimal impact on red blood cell integrity and low toxicity to erythrocytes. The cytotoxicity assays revealed IC_{50} values greater than 18 μM for all compounds, suggesting low cytotoxicity and indicating that these compounds can potentially exhibit antimicrobial activity without causing significant damage to host cells, Table 2.

First, the interaction analysis between the phenyltriazole **23** analog and dihydropteroate synthase (DHPS) reveals several similarities and differences compared to the reference bound Pterin–sulfa conjugate. Key insights into these interactions are derived from the analysis of hydrogen bonding, ionic interactions, and π-interactions with the receptor residues. First of all, both the phenyltriazole analog **23** and Pterin–sulfa conjugate engages in strong hydrogen bonding with conserved residues in DHPS, specifically **ASN 103** and **ASP 167**. The analog shows hydrogen bond interactions with **ASN 103** at 2.83 Å and $E = -4.3$ kcal mol^{-1} and **ASP 167** at 2.73 Å, $E = -5.9$ kcal mol^{-1}, which are similar to the interactions seen in the reference substrate with **ASN 103** at 3.02 Å, $E = -4.3$ kcal mol^{-1} and **ASP 167** at 2.87 Å, $E = -6.7$ kcal mol^{-1}. This suggests that these residues play a central role in stabilizing the ligand in both cases, with particularly strong interactions between the analog and **ASP 167**, reflected in a highly favorable binding energy. In addition, it also forms hydrogen bonds with **SER 16** at 2.95 Å, $E = -3.4$ kcal mol^{-1} and **LYS 203** at 3.17 Å, $E = -8.9$ kcal mol^{-1}, whereas the bound inhibitor forms hydrogen bonds with **LYS 203** at 3.71 Å, $E = -1.7$ kcal mol^{-1} which suggests a more favorable fit for the analog at this binding site. Both the **23** and reference bound compound formed an ionic interaction with **ASP 84** and **ASP 167**; (2.83 Å, $E = -3.3$ kcal mol^{-1}) and (2.84 Å, $E = -4.9$ kcal mol^{-1}) and (3.78 Å, $E = -1.0$ kcal mol^{-1}) (3.88 Å, $E = -0.7$ kcal mol^{-1}) respectively. Moreover, both the analog **23** and Pterin–sulfa conjugate show π-interactions with **LYS 203** and **PHE 172** through the aromatic fragments, which in turn is less energetically significant than hydrogen bonding or ionic interactions but still contributes to ligand stability. In conclusion, the phenyltriazole analog forms similar interactions with DHPS as the reference substrate, with notable improvements in the binding affinity for **LYS 203** and **ASP 167** (Fig. 7).

2.3.2 Computational ADME analysis. Predicting pharmacokinetic and pharmacodynamic properties plays a crucial role in the drug development process, as it enables researchers to decide whether to optimize a lead compound or move on to alternative candidates. Over the past 20 years,[55] various online tools and software have been created to estimate key ADME

Table 2 The prediction screen of binding data and inhibition constant of selected compounds against MRSA targets (K_i (nM))[a]

	PBP2a		DHPS				
Cp.	ΔG (kcal mol^{-1})	K_i (nM)	ΔG (kcal mol^{-1})	K_i (nM)	Hemolysis LC [mg mL^{-1}]	PSA [Å^2]	HEK293 cytotoxicity IC_{50} [μM]
23	−8.16	33.25	−8.54	26.91	>10	149	52.4
24	−7.99	34.67	−8.12	30.55	>10	148	18.9

[a] Two targets from methicillin-resistant *Staphylococcus aureus*; G acyl-penicillin binding protein 2a (PDB ID: 1MWT) and dihydropteroate synthase (PDB ID: 6CLV). MTT assay for cytotoxicity against human embryonic kidney cell line. LC lytic concentration 30%.

 © 2025 The Author(s). Published by the Royal Society of Chemistry

Open Access Article. Published on 17 June 2025. Downloaded on 11/7/2025 8:09:35 PM.
This article is licensed under a Creative Commons Attribution-NonCommercial 3.0 Unported Licence.

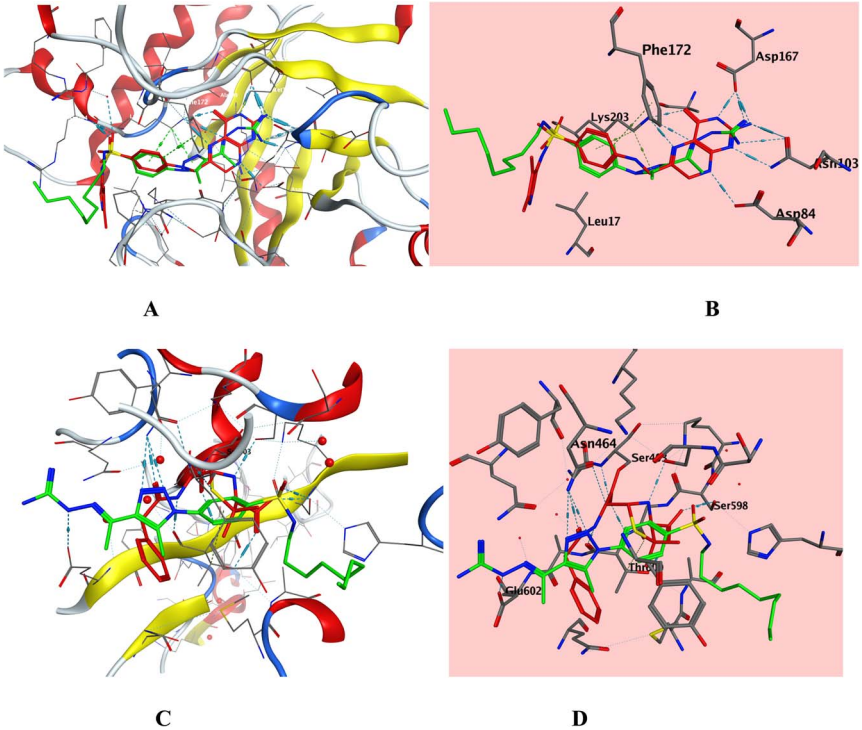

Fig. 7 Target enzymes interaction map (A and B) bound ligand and **23** within dihydropteroate synthase (PDB ID: 6CLV), (C and D) bound ligand and **23** within G acyl-penicillin binding protein 2a (PDB ID: 1MWT).

(absorption, distribution, metabolism, and excretion) parameters. In this study, we evaluated the ADME profiles of the three most promising compounds from our library, with the results presented in Tables 3 and 4. To assess their ADME characteristics, structural similarity, and physicochemical properties, we utilized three computational platforms: PreADME, SwissADME, and Molsoft.

The molecular weights of the selected compounds are all below 500, their log *P* values (octanol/water partition coefficient) are under 5, and they possess fewer than 5 hydrogen bond donors and acceptors. Based on these characteristics, compounds **23** and **24** are expected to exhibit good absorption. Additionally, the number of rotatable bonds as an indicator of molecular flexibility and a factor influencing oral bioavailability was analyzed. This value is determined by counting non-ring, non-terminal, non-hydrogen-bonded single bonds, and is categorized into three groups: ≤7, 8–10, and >10. Compound **24** has **8** rotatable bonds, indicating generally favorable bioavailability, while compound **23**, with 14 rotatable bonds, suggests moderate bioavailability. All three candidates have fewer than 5 hydrogen bond donors, and compounds **23** and **24** each have 7 hydrogen bond acceptors. These findings support the potential for good absorption in all three compounds.[57]

All three compounds have identical values for tPSA (159.52), hydrogen bond donors,[4] and hydrogen bond acceptors,[7]

Table 3 Physiochemical properties prediction through SwissADME[56]

Code	tPSA[a]	H-bond donor	H-bond acceptor	NORTB[b]	MW[c]	Log *P*
23	159.52	4	7	14	462.61	3.08
24	159.52	4	7	8	392.48	1.23

[a] TPSA, topological polar surface area. [b] NORTB, number of rotatable bonds. [c] MW, molecular weight.

Table 4 Predicting drug-likeness using Molosoft[55] and SwissADME

Code	Solubility (mg L^{-1})	Drug likeness model score	Lipinski's rule violation	Bioavailability score
23	1.3	0.33	0	0.55
24	4.83	0.98	0	0.55

Open Access Article. Published on 17 June 2025. Downloaded on 11/7/2025 8:09:35 PM.
This article is licensed under a Creative Commons Attribution-NonCommercial 3.0 Unported Licence.

indicating similar polarity and hydrogen bond formation potential. However, they differ in the number of rotatable bonds (NORTB), molecular weight (MW), and log *P* values. Compound **23** has the highest NORTB,[14] MW (462.61), and log *P* (3.08), suggesting greater flexibility, higher molecular mass, and higher lipophilicity compared to the others. While compound **24** has lower NORTB,[8] lower MW, and lower log *P* values (1.23), suggesting that they are less flexible and less lipophilic than compound **23**. This suggests that despite having similar hydrogen bonding capabilities, the structural differences between the compounds (in terms of flexibility and lipophilicity) could influence their pharmacokinetic behavior. On the other hand, Table 4 shows the predicted drug-like properties of three compounds (**23** and **24**) using Molsoft and SwissADME. The data shows different solubility levels, with compound **23** displaying the lowest solubility (1.3 mg L^{-1}), while compound **24** has higher solubility values of 4.83 mg L^{-1}. Notably, compound **24** exhibits the highest drug-like value in the model (0.98), followed by compound **23** (0.33), indicating that compound **24** has the most favorable drug-like properties. The two compounds meet Lipinski's rule, without violations, suggesting good potential for oral bioavailability. The bioavailability value is consistent for all compounds and is, with a value of 0.55 for all. Overall, compound **24** stands out as the most promising candidate due to its high solubility and superior drug likeness, making it a favorable candidate for further development.

Table 5 summarizes the predicted pharmacokinetic properties of compounds **23**, **24**, and the reference drug vancomycin using pre-ADME analysis. Notably, compound **24** and vancomycin have much lower BBB penetration (0.06 and 0.03, respectively), which indicates limited access to central nervous system. Regarding Caco-2 permeability, vancomycin exhibits a much higher rate (20.64×10^6 cm s^{-1}) compared to all three test compounds, indicating better intestinal absorption. However, compound **23** shows moderate permeability (1.07×10^6 cm s^{-1}), surpassing compound **24**. All compounds show good human intestinal absorption (HIA), with compound **23** being the highest at 70.1% HIA achieved, and also plasma protein binding (PPB) is highest (84.25%), which may influence its bioavailability and distribution, while compound **24** shows the lowest PPB at 52.1%.

All test compounds function as CYP2D6 substrates, unlike vancomycin, which does not interact with this enzyme.

2.4 Prediction of toxicity

Predicting the toxicity of a compound is a critical step in the development of new drug candidates, making *in silico* toxicity studies a faster and cheaper procedure than *in vivo* animal toxicity testing or *in vitro* testing in cell lines. It also helps significantly reduce the number of animals used in experimental assays. Several online programs access toxicities that use *in silico* models to predict mean lethal dose, carcinogenicity, mutagenicity, and more.

The Pro-Tox II web server[58] predicts the mean lethal dose (LD_{50}) in rodents. According to this program, all compounds can be classified into six GHS (Globally Harmonized System of Classification and Labeling of Chemicals) Categories[59] according to their toxicity and LD_{50} value.

Toxicity classes are defined according to the globally harmonized system of classification of labeling of chemicals (GHS). LD_{50} was noted in mg kg^{-1} units.

- Class I: fatal if swallowed ($LD_{50} \leq 5$)
- Class II: fatal if swallowed ($5 < LD_{50} \leq 50$)
- Class III: toxic if swallowed ($50 < LD_{50} \leq 300$)
- Class IV: harmful if swallowed ($300 < LD_{50} \leq 2000$)
- Class V: may be harmful if swallowed ($2000 < LD_{50} \leq 5000$)
- Class VI: non-toxic ($LD_{50} > 5000$)

Toxicity assessment is an important part of the development of therapeutic agents as it directly impacts their safety profile and potential clinical applications (Table 6) reveals critical insights into the predicted toxicity of the listed compounds. All three compounds (**23** and **24**) have the same predicted LD_{50} value of 500 mg kg^{-1}, and are therefore classified in toxicity class IV, which indicates low toxicity. However, there are clear differences in their specific toxicity profiles. Compound **24** was predicted to have active carcinogenicity with values of 0.59, while compound **23** shows a slightly lower activity (0.55). In contrast, two compounds show inactivity regarding hepatotoxicity, mutagenicity, and cytotoxicity, although the values indicate slight differences in their relative safety. While the compounds exhibit low toxicity overall, the Table 6 highlights the importance of evaluating toxicity when developing new compounds. Compound **23** appears to be the most promising candidate in terms of safety, while compound **24** may require further investigation to address their active toxicity profiles. Understanding these factors is crucial for advancing these compounds toward therapeutic applications.

Table 5 Pharmacokinetics prediction through pre-ADME

	Pharmacokinetics					
Code	BBB[a]	CACO-2[b] ($\times 10^6$ cm s^{-1})	HIA[c] (%)	MDCK[d] (nm s^{-1})	PPB[e] (%)	CYP2D6[f]
23	0.21	1.07	70.10	0.08	84.25	Substrate
24	0.06	0.38	60.01	12.33	52.10	Substrate
Vancomycin	0.0.26	20.59	1.19	0.039	42.18	No

[a] BBB: blood–brain barrier penetration. [b] CACO-2: permeability through cells derived from human colon adenocarcinoma. [c] HIA: percentage human intestinal absorption. [d] MDCK: permeability through Madin–Darby canine kidney cells. [e] PPB: plasma protein binding. [f] CYP2D6: cytochrome P450 2D6.

 © 2025 The Author(s). Published by the Royal Society of Chemistry

Open Access Article. Published on 17 June 2025. Downloaded on 11/7/2025 8:09:35 PM. This article is licensed under a Creative Commons Attribution-NonCommercial 3.0 Unported Licence.

Table 6 Prediction of toxicity

No	Predicted LD_{50} (mg kg^{-1})	Predicted toxicity class	Hepatotoxicity	Carcinogenicity	Mutagenicity	Cytotoxicity
23	500	IV	Inactive (0.63)	Active (0.55)	Inactive (0.54)	Inactive (0.55)
24	500	IV	Inactive (0.68)	Active (0.59)	Inactive (0.59)	Inactive (0.59)

3. Conclusion

Bacterial infections remain a significant challenge in the medical field due to the rapid development of bacterial resistance to existing antibacterial agents. Therefore, there is an urgent need to continuously discover new scaffolds of antimicrobial agents to combat these infections. While sulfonamides have limited activity against methicillin-resistant *Staphylococcus aureus* (MRSA), our laboratory has already developed antibacterial agents from phenyltriazoles that are specifically effective against MRSA. The synthesis and biological evaluation of phenyltriazole–sulfonamide hybrids have led to the identification of several promising compounds with significant antimicrobial activity, particularly against MRSA. The structure–activity relationship (SAR) analysis revealed that modifications in alkyl chain length and branching, along with functional group variations, significantly influenced the antimicrobial potency of these compounds. In this study, we found that analog **23** showed even better results with an MIC of 1 μg ml^{-1} against *Staphylococcus aureus* USA300, indicating that the addition of a nonyl group gave the best results. However, compound **24** showed good activity against *Acinetobacter baumannii* AB5075, with a minimum inhibitory concentration (MIC) of 8 μg ml^{-1}. Compound **23**, featuring an *n*-nonyl group, demonstrated the best antimicrobial performance, exhibiting rapid bactericidal activity and effective disruption of MRSA biofilms that outperformed reference vancomycin drug. *In silico* studies further supported the potential of these compounds to target key enzymes involved in bacterial survival, including PBP2a and DHPS, with favorable binding affinities. These findings suggest that phenyltriazole–sulfonamide hybrids could serve as viable alternatives or complements to existing antibiotics, particularly in addressing drug-resistant infections. Further research and optimization of these compounds could lead to the development of novel therapies to combat resistant bacterial pathogens and biofilm-related infections.

4. Experimental section

4.1 Chemistry

^{1}H NMR (400 MHz) and ^{13}C NMR (100 MHz) spectra were recorded in $CDCl_3$ or DMSO-d_6 using a Varian Mercury VX-400 spectrometer. Chemical shifts (δ, ppm) were referenced to solvent peaks. Flash chromatography was carried out on 230–400 mesh silica, and reaction progress was monitored using Merck silica gel IB2-F plates (0.25 mm). Mass spectra were obtained at 70 eV, and high-resolution mass spectra were recorded on a Finnigan MAT XL95. MIC values for the compounds and linezolid (control) were determined at the Department of Microbiology and Immunology, Faculty of Pharmacy, Cairo University. Melting points were measured with a Stuart SMP30 apparatus using capillary tubes and are uncorrected. Reported yields correspond to isolated products.

4-Azidobenzenesulfonamide **2** was prepared as reported procedures.[23]

4.1.1 4-(4-Acetyl-5-methyl-1*H*-1,2,3-triazol-1yl) benzenesulfonamide 3. General procedure: compound **2** was dissolved in ethanol. Acetyl acetone (5 equiv.) and sodium ethoxide (2 equiv.) were added. The reaction was stirred for 4–6 hours on reflux temperature. The white solid was precipitated in the reaction flask. Therefore, the reaction mixture was allowed to cool, filtered. The solution was then poured on cold water to obtain the rest of the yield as white solid precipitate in solution compound **3**.

4.1.2 Synthesis of different triazole derivatives 4–15. General procedure: compound **3** was dissolved in DMF as a solvent, K_2CO_3 (2 equiv.) and different alkylhalides (2 equiv.) were added. The reaction was stirred for 1 hour at 75 °C. Monitor with TLC till the disappearance of the start spot completely. The reaction mixture was allowed to cool down, poured on cold water to obtain the white solid precipitate of compounds **4–15**, which was then filtered and allowed to dry. The product material was a mixture of both mono-alkylated and di-alkylated compounds, so the crude products were purified by silica gel flash chromatography using hexane–ethyl acetate (9 : 1) and then washed. Yields, physical properties, and spectral data of the purified compounds are provided below.

*4.1.2.1 4-(4-Acetyl-5-methyl-1H-1,2,3-triazol-1-yl)-N-methylbenzenesulfonamide **4**.* White solid (286 mg, 84%). mp = 115–116 °C; ^{1}H NMR-DMSO-d6, δ: 8.01 (d, J = 8.1 Hz, 2H), 7.92 (d, J = 8.1 Hz, 2H), 7.86 (brs, 1H), 2.71 (s, 3H), 2.56 (s, 3H), 2.37 (s, 3H); ^{13}C NMR (DMSO-d_6) δ: 199.70, 145.25, 139.67, 139.19, 136.01, 131.53, 129.51, 126.33, 29.17, 14.89, 11.54; anal. calc. for: $C_{12}H_{14}N_4O_3S$ (294): C, 48.97; H, 4.79; N, 19.04%; found: C, 49.08; H, 4.86; N, 18.94%.

*4.1.2.2 4-(4-Acetyl-5-methyl-1H-1,2,3-triazol-1-yl)-N-ethylbenzenesulfonamide **5**.* Buff solid (203 mg, 82%). mp = 117–119 °C; ^{1}H NMR-DMSO-d6, δ: 8.05 (d, J = 8.1 Hz, 2H), 7.87 (d, J = 8.1 Hz, 2H), 7.80 (brs, 1H), 2.9 (q, J = 8.0 Hz, 2H), 2.54 (s, 3H), 2.37 (s, 3H), 1.05 (t, J = 8.0 Hz, 3H); ^{13}C NMR (DMSO-d_6) δ: 194.40, 154.88, 145.19, 141.76, 139.10, 135.22, 131.48, 128.44, 126.31, 120.46, 38.00, 14.90, 11.50, 9.99; anal. calc. for: $C_{13}H_{16}N_4O_3S$ (308): C, 50.64; H, 5.23; N, 18.17%; found: C, 50.71; H, 5.31; N, 18.05%.

*4.1.2.3 4-(4-Acetyl-5-methyl-1H-1,2,3-triazol-1-yl)-N-butylbenzenesulfonamide **6**.* White solid (322 mg, 81%). mp = 116–118 °C; ^{1}H NMR-DMSO-d6, δ: 8.03 (d, J = 8.1 Hz, 2H), 7.87 (d, J = 8.1 Hz, 2H), 7.76 (brs, 1H), 2.84 (t, J = 8.1 Hz, 2H), 2.54 (s, 3H),

Open Access Article. Published on 17 June 2025. Downloaded on 11/7/2025 8:09:35 PM. This article is licensed under a Creative Commons Attribution-NonCommercial 3.0 Unported Licence.

2.37 (s, 3H), 1.42–1.21 (m, 4H), 0.83 (t, J = 8.0 Hz, 3H); ^{13}C NMR (DMSO-d_6) δ: 199.34, 145.24, 144.43, 141.82, 139.07, 131.42, 128.41, 126.30, 42.73, 31.57, 19.64, 14.88, 13.92, 11.49; anal. calc. for: $C_{15}H_{20}N_4O_3S$ (336): C, 53.56; H, 5.99; N, 16.65%; found: C, 53.59; H, 6.07; N, 16.54%.

4.1.2.4 4-(4-Acetyl-5-methyl-1H-1,2,3-triazol-1-yl)-N-pentylbenzenesulfonamide 7. White solid (261 mg, 85%). mp = 119–120 °C; ^{1}H NMR-DMSO-d6, δ: 8.03 (d, J = 8.1 Hz, 2H), 7.87 (d, J = 8.1 Hz, 2H), 7.74 (brs, 1H), 2.84 (t, J = 8.1 Hz, 2H), 2.54 (s, 3H), 2.37 (s, 3H), 1.43–1.19 (m, 6H), 0.83 (t, J = 8.0 Hz, 3H); ^{13}C NMR (DMSO-d_6) δ: 200.85, 145.17, 144.57, 141.88, 139.06, 131.48, 128.42, 126.29, 43.01, 29.13, 28.67, 22.08, 14.90, 14.26, 11.48; anal. calc. for: $C_{16}H_{22}N_4O_3S$ (350): C, 54.84; H, 6.33; N, 15.99%; found: C, 54.94; H, 6.39; N, 15.89%.

*4.1.2.5 4-(4-Acetyl-5-methyl-1H-1,2,3-triazol-1-yl)-N-hexylbenzenesulfonamide **8**.* White solid (392 mg, 88%). mp = 120–121 °C; ^{1}H NMR-DMSO-d6, δ: 8.03 (d, J = 8.1 Hz, 2H), 7.87 (d, J = 8.1 Hz, 2H), 7.76 (brs, 1H), 2.84 (t, J = 8.0 Hz, 2H), 2.51 (s, 3H), 2.37 (s, 3H), 1.49–1.14 (m, 8H), 0.86 (t, J = 8.0 Hz, 3H); ^{13}C NMR (DMSO-d_6) δ: 192.48, 145.20, 141.88, 139.06, 131.45, 128.42, 128.23, 126.28, 120.43, 43.05, 31.19, 29.40, 29.30, 26.10, 22.39, 14.89, 14.30, 11.48; anal. calc. for: $C_{17}H_{24}N_4O_3S$ (364): C, 56.02; H, 6.64; N, 15.37%; found: C, 56.22; H, 6.76; N, 15.17%.

*4.1.2.6 4-(4-Acetyl-5-methyl-1H-1,2,3-triazol-1-yl)-N-heptylbenzenesulfonamide **9**.* White solid (324 mg, 83%). mp = 119–120 °C; ^{1}H NMR-DMSO-d6 δ: 8.04 (d, J = 8.1 Hz, 2H), 7.86 (d, J = 8.1 Hz, 2H), 7.27 (brs, 1H), 3.15 (t, J = 8.1 Hz, 2H), 2.55 (s, 3H), 2.41 (s, 3H), 1.51–1.21 (m, 10H), 0.86 (t, J = 8.0 Hz, 3H); ^{13}C NMR (DMSO-d_6) δ: 196.81, 145.33, 144.62, 141.96, 138.95, 131.99, 128.45, 128.23, 126.31, 43.04, 31.56, 29.44, 28.65, 26.39, 22.44, 15.07, 14.35, 11.43; anal. calc. for: $C_{18}H_{26}N_4O_3S$ (378): C, 57.12; H, 6.92; N, 14.80%; found: C, 57.22; H, 6.99; N, 14.70%.

*4.1.2.7 4-(4-Acetyl-5-methyl-1H-1,2,3-triazol-1-yl)-N-octylbenzenesulfonamide **10**.* Pale white solid (357 mg, 84%). mp = 120–122 °C; ^{1}H NMR-DMSO-d6 δ: 8.05 (d, J = 8.1 Hz, 2H), 7.86 (d, J = 8.1 Hz, 2H), 7.27 (brs, 1H), 2.84 (t, J = 8.1 Hz, 2H), 2.56 (s, 3H), 2.49 (s, 3H), 1.40–1.35 (m, 2H), 1.26–1.19 (m, 10H), 0.85 (t, J = 8.0 Hz, 3H); ^{13}C NMR (DMSO-d_6) δ: 193.80, 147.36, 143.17, 142.19, 138.69, 133.36, 128.5, 126.4, 43.04, 31.62, 29.47, 28.95, 26.45, 22.51, 15.52, 14.38, 11.31; anal. calc. for: $C_{19}H_{28}N_4O_3S$ (392): C, 58.14; H, 7.19; N, 14.27%; found: C, 58.24; H, 7.29; N, 14.17%.

*4.1.2.8 4-(4-Acetyl-5-methyl-1H-1,2,3-triazol-1-yl)-N-nonylbenzenesulfonamide **11**.* Buff solid (271 mg, 72%). mp = 122–123 °C; ^{1}H NMR-DMSO-d6 δ: 8.06 (d, J = 8.1 Hz, 2H), 7.89 (d, J = 8.1 Hz, 2H), 7.76 (brs, 1H), 2.84 (t, J = 8.1 Hz, 2H), 2.56 (s, 3H), 2.54 (s, 3H), 1.42–1.36 (m, 2H), 1.23–1.19 (m, 12H), 0.85 (t, J = 8.0 Hz, 3H); ^{13}C NMR (DMSO-d_6) δ: 186.20, 148.33, 142.40, 142.31, 138.55, 134.09, 128.55, 126.47, 43.04, 31.70, 29.45, 29.30, 28.99, 26.43, 22.52, 15.95, 14.39, 11.24; anal. calc. for: $C_{20}H_{30}N_4O_3S$ (406): C, 59.09; H, 7.44; N, 13.78%; found: C, 59.29; H, 7.54; N, 13.68%.

*4.1.2.9 4-(4-Acetyl-5-methyl-1H-1,2,3-triazol-1-yl)-N-isobutylbenzenesulfonamide **12**.* White solid (204 mg, 85%). mp = 121–122 °C; ^{1}H NMR-DMSO-d6 δ: 8.03 (d, J = 8.0 Hz, 2H), 7.87 (d, J = 8.0 Hz, 2H), 7.84 (brs, 1H), 2.65 (d, J = 8.0 Hz, 2H), 2.54 (s, 3H), 2.37 (s, 3H), 1.71 (m, 1H), 0.85 (d, J = 8.0 Hz, 6H); ^{13}C NMR (DMSO-d_6) δ: 194.37, 144.48, 141.94, 139.04, 131.44, 128.38, 126.29, 50.5, 28.59, 20.32, 14.89, 11.51; anal. calc. for: $C_{15}H_{20}N_4O_3S$ (336): C, 53.56; H, 5.99; N, 16.65%; found: C, 53.60; H, 6.05; N, 16.60%.

*4.1.2.10 4-(4-Acetyl-5-methyl-1H-1,2,3-triazol-1-yl)-N-(5-methylhexyl)benzenesulfonamide **13**.* Buff solid (284 mg, 83%). mp = 122–123 °C; ^{1}H NMR-DMSO-d6, δ: 8.03 (d, J = 8.1 Hz, 2H), 7.86 (d, J = 8.1 Hz, 2H), 7.27 (brs, 1H), 2.95–2.67 (m, 1H), 2.54 (s, 3H), 2.38 (s, 3H), 1.67–1.09 (m, 8H), 0.86 (t, J = 8.0 Hz, 3H); ^{13}C NMR (DMSO-d_6) δ: 193.03, 144.78, 142.04, 138.98, 131.63, 128.39, 126.30, 49.21, 37.77, 30.71, 30.54, 26.37, 25.72, 14.94, 11.46; anal. calc. for: $C_{18}H_{26}N_4O_3S$ (378): C, 57.12; H, 6.92; N, 14.80%; found: C, 57.22; H, 6.99; N, 14.69%.

*4.1.2.11 4-(4-Acetyl-5-methyl-1H-1,2,3-triazol-1-yl)-N-(but-3-en-1-yl)benzenesulfonamide **14**.* White solid (254 mg, 86%). mp = 111–112 °C; ^{1}H NMR-DMSO-d6 δ: 8.04 (d, J = 8.1 Hz, 2H), 7.87 (d, J = 8.1 Hz, 2H), 7.85 (brs, 1H), 5.79–5.68 (m, 2H), 5.01 (dd, J = 12.0 Hz, 2H), 2.92 (t, J = 8.0 Hz, 2H), 2.52 (s, 3H), 2.38 (s, 3H), 2.19–2.14 (m, 2H); ^{13}C NMR (DMSO-d_6) δ: 195.49, 144.77, 141.76, 139.09, 135.68, 131.63, 128.46, 126.32, 117.27, 42.62, 33.92, 14.93, 11.49; anal. calc. for $C_{15}H_{18}N_4O_3S$ (334): C, 53.88; H, 5.43; N, 16.76%; found: C, 53.94; H, 5.48; N, 16.70%.

*4.1.2.12 4-(4-Acetyl-5-methyl-1H-1,2,3-triazol-1-yl)-N-cyclopentylbenzenesulfonamide **15**.* Buff solid (273 mg, 83%). mp = 129–130 °C; ^{1}H NMR-DMSO-d6 δ: 8.05 (d, J = 8.1 Hz, 2H), 8.03 (brs, 1H), 7.86 (d, J = 8.1 Hz, 2H), 3.52–3.48 (m, 1H), 2.54 (s, 3H), 2.37 (s, 3H), 1.68–1.34 (m, 8H); ^{13}C NMR (DMSO-d_6) δ: 195.13, 145.22, 144.46, 142.77, 139.01, 131.42, 128.43, 126.26, 55.02, 32.95, 23.28, 14.89, 11.53; anal. calc. for: $C_{16}H_{20}N_4O_3S$ (348): C, 55.16; H, 5.79; N, 16.08%; found: C, 55.21; H, 5.85; N, 16.01%.

4.1.3 Addition of aminoguanidine to different triazole derivatives (15–27). General procedure: both mono and di-alkylated triazole acetyl compounds (**4–15**) were dissolved in ethanol after that 1 ml of conc. hydrochloric acid and (2 equiv.) of aminoguanidine bicarbonate was added. The reaction mixture was heated under reflux with stirring and monitored with TLC for the complete disappearance of the start spot. The reaction mixture was added to cold water to give the white solid powder of final products. Yields, physical properties, and spectral data of isolated purified products are listed below.

*4.1.3.1 2-(1-(5-Methyl-1-(4-(N-methylsulfamoyl)phenyl)-1H-1,2,3-triazol-4-yl)ethylidene) hydrazine-1-carboximidamide **16**.* White solid (322 mg, 88%). mp = 162–163 °C; ^{1}H NMR-DMSO-d6 δ: 8.01 (d, J = 8.1 Hz, 2H), 7.92 (d, J = 8.1 Hz, 2H), 7.86 (brs. 1H), 5.67 (brs, 4H), 2.71 (s, 3H), 2.56 (s, 3H), 2.37 (s, 3H); ^{13}C NMR (DMSO-d_6) δ: 145.25, 139.67, 139.19, 136.01, 131.43, 129.51, 126.33, 29.17, 14.89, 11.54; anal. calc. for: $C_{13}H_{18}N_8O_2S$ (350.40): C, 44.56; H, 5.18; N, 31.98%; found: C, 44.66; H, 5.28; N, 31.88%.

*4.1.3.2 2-(1-(1-(4-(N-Ethylsulfamoyl)phenyl)-5-methyl-1H-1,2,3-triazol-4-yl)ethylidene)hydrazine-1-carboximidamide **17**.* Buff solid (276 mg, 85%). mp = 160–161 °C; ^{1}H NMR-DMSO-d6 δ: 8.05 (d, J = 8.1 Hz, 2H), 7.87 (d, J = 8.1 Hz, 2H), 7.77 (brs, 1H), 5.83 (brs, 4H), 2.90 (q, J = 8.0 Hz, 2H), 2.56 (s, 3H), 2.37 (s, 3H), 1.07 (t, J = 8.0 Hz, 3H); ^{13}C NMR (DMSO-d_6) δ: 162.85, 160.77, 159.89, 154.88, 145.19, 144.53, 141.76, 139.10, 135.22, 131.66, 128.44, 126.31, 120.46, 38.11, 17.74, 15.27, 11.50, 9.99; anal.

 © 2025 The Author(s). Published by the Royal Society of Chemistry

Open Access Article. Published on 17 June 2025. Downloaded on 11/7/2025 8:09:35 PM. This article is licensed under a Creative Commons Attribution-NonCommercial 3.0 Unported Licence.

calc. for: $C_{14}H_{20}N_8O_2S$ (364.43): C, 46.14; H, 5.53; N, 30.75%; found: C, 46.34; H, 5.75; N, 30.55%.

4.1.3.3 2-(1-(1-(4-(N-Butylsulfamoyl)phenyl)-5-methyl-1H-1,2,3-triazol-4-yl)ethylidene)hydrazine-1-carboximidamide ***18.*** White solid (393 mg, 89%). mp = 169–171 °C; ^{1}H NMR-DMSO-d6 δ: 8.03 (d, J = 8.1 Hz, 2H), 7.87 (d, J = 8.1 Hz, 2H), 5.69 (brs, 5H), 2.84 (t, J = 8.1 Hz, 2H), 2.54 (s, 3H), 2.37 (s, 3H), 1.42–1.21 (m, 4H), 0.83 (t, J = 8.0 Hz, 3H); ^{13}C NMR (DMSO-d_6) δ: 159.98, 145.24, 144.43, 141.82, 139.07, 131.42, 128.41, 126.30, 42.73, 31.57, 19.64, 14.88, 13.92, 11.49; anal. calc. for: $C_{16}H_{24}N_8O_2S$ (392.48): C, 48.96; H, 6.16; N, 28.55%; found: C, 49.06; H, 6.26; N, 28.35%.

4.1.3.4 2-(1-(5-Methyl-1-(4-(N-pentylsulfamoyl)phenyl)-1H-1,2,3-triazol-4-yl)ethylidene) hydrazine-1-carboximidamide ***19.*** White solid (326 mg, 90%). mp = 162–163 °C; ^{1}H NMR-DMSO-d6 δ: 8.03 (d, J = 8.1 Hz, 2H), 7.87 (d, J = 8.1 Hz, 2H), 5.69 (brs, 5H), 2.84 (t, J = 8.1 Hz, 2H), 2.54 (s, 3H), 2.37 (s, 3H), 1.43–1.19 (m, 6H), 0.83 (t, J = 8.0 Hz, 3H); ^{13}C NMR (DMSO-d_6) δ: 159.87, 145.17, 144.57, 141.88, 139.06, 131.48, 128.42, 126.29, 43.01, 29.13, 28.67, 28.62, 22.08, 14.90, 14.26, 11.48; anal. calc. for: $C_{17}H_{26}N_8O_2S$ (406.51): C, 50.23; H, 6.45; N, 27.57%; found: C, 50.43; H, 6.55; N, 27.37%.

4.1.3.5 2-(1-(1-(4-(N-Hexylsulfamoyl)phenyl)-5-methyl-1H-1,2,3-triazol-4-yl)ethylidene)hydrazine-1-carboximidamide ***20.*** White solid (441 mg, 90%). mp = 163–165 °C; ^{1}H NMR-DMSO-d6 δ: 8.03 (d, J = 8.1 Hz, 2H), 7.87 (d, J = 8.1 Hz, 2H), 7.76 (brs, 1H), 5.81 (brs, 4H), 2.84 (t, J = 8.0 Hz, 2H), 2.51 (s, 3H), 2.37 (s, 3H), 1.49–1.14 (m, 8H), 0.86 (t, J = 8.0 Hz, 3H); anal. calc. for: $C_{18}H_{28}N_8O_2S$ (420.54): C, 51.41; H, 6.71; N, 26.65%; found: C, 51.61; H, 6.81; N, 26.55%.

4.1.3.6 2-(1-(1-(4-(N-Heptylsulfamoyl)phenyl)-5-methyl-1H-1,2,3-triazol-4-yl)ethylidene hydrazine-1-carboximidamide ***21.*** White solid (449 mg, 87%). mp = 160–162 °C; ^{1}H NMR-DMSO-d6 δ: 8.04 (d, J = 8.1 Hz, 2H), 7.86 (d, J = 8.1 Hz, 2H), 7.74 (brs, 1H), 6.14 (brs, 4H), 2.83 (t, J = 8.1 Hz, 2H), 2.57 (s, 3H), 2.41 (s, 3H), 1.42–1.19 (m, 10H), 0.85 (t, J = 8.0 Hz, 3H); anal. calc. for: $C_{19}H_{30}N_8O_2S$ (434.56): C, 52.51; H, 6.96; N, 25.79%; found: C, 52.55; H, 7.05; N, 25.59%.

4.1.3.7 2-(1-(5-Methyl-1-(4-(N-octylsulfamoyl)phenyl)-1H-1,2,3-triazol-4-yl)ethylidene)hydrazine-1-carboximidamide ***22.*** Pale-white solid (465 mg, 88%). mp = 174–176 °C; ^{1}H NMR-DMSO-d6 δ: 8.05 (d, J = 8.1 Hz, 2H), 7.86 (d, J = 8.1 Hz, 2H), 7.27 (brs, 5H), 2.84 (t, J = 8.1 Hz, 2H), 2.56 (s, 3H), 2.49 (s, 3H), 1.40–1.35 (m, 2H), 1.26–1.19 (m, 10H), 0.85 (t, J = 8.0 Hz, 3H); ^{13}C NMR (DMSO-d_6) δ: 157.38, 147.36, 143.17, 142.19, 138.69, 133.36, 128.5, 126.4, 43.04, 31.62, 29.47, 29.01, 28.95, 26.45, 22.51, 15.52, 14.38, 11.31; anal. calc. for: $C_{20}H_{32}N_8O_2S$ (448.59): C, 53.55; H, 7.19; N, 24.98%; found: C, 53.75; H, 7.29; N, 24.88%.

4.1.3.8 2-(1-(5-Methyl-1-(4-(N-nonylsulfamoyl)phenyl)-1H-1,2,3-triazol-4-yl)ethylidene)hydrazine-1-carboximidamide ***23.*** Buff solid (305 mg, 74%). mp = 165–166 °C; ^{1}H NMR-DMSO-d6 δ: 11.46 (brs, 1H), 8.06 (d, J = 8.1 Hz, 2H), 7.89 (d, J = 8.1 Hz, 2H), 7.76 (brs, 4H), 2.84 (t, J = 8.1 Hz, 2H), 2.56 (s, 3H), 2.54 (s, 3H), 1.42–1.36 (m, 2H), 1.23–1.19 (m, 12H), 0.85 (t, J = 8.0 Hz, 3H); ^{13}C NMR (DMSO-d_6) δ: 156.61, 148.33, 142.40, 142.31, 138.55, 134.09, 128.55, 126.47, 43.04, 31.70, 29.45, 29.30, 29.05, 28.99, 26.43, 22.52, 15.95, 14.39, 11.24; anal. calc. for: $C_{21}H_{34}N_8O_2S$ (462.62): C, 54.52; H, 7.41; N, 24.22%; found: C, 54.71; H, 7.51; N, 24.02%.

4.1.3.9 2-(1-(1-(4-(N-Isobutylsulfamoyl)phenyl)-5-methyl-1H-1,2,3-triazol-4-yl)ethylidene) hydrazine-1-carboximidamide ***24.*** White solid (270 mg, 90%). mp = 161–163 °C; ^{1}H NMR-DMSO-d6 δ: 8.03 (d, J = 8.0 Hz, 2H), 7.87 (d, J = 8.0 Hz, 2H), 5.68 (brs, 5H), 2.65 (d, J = 8.0 Hz, 2H), 2.54 (s, 3H), 2.37 (s, 3H), 1.71 (m, 1H), 0.85 (d, J = 8.0 Hz, 6H); ^{13}C NMR (DMSO-d_6) δ: 159.91, 145.2, 144.48, 141.94, 139.04, 131.44, 128.38, 126.29, 50.5, 28.59, 20.32, 14.89, 11.51; anal. calc. for: $C_{16}H_{24}N_8O_2S$ (392.48): C, 48.96; H, 6.16; N, 28.55%; found: C, 49.06; H, 6.28; N, 28.35%.

4.1.3.10 2-(1-(5-Methyl-1-(4-(N-(5-methylhexyl)sulfamoyl) phenyl)-1H-1,2,3-triazol-4-yl)ethylidene) hydrazine-1-carboximidamide ***25.*** Buff solid (329 mg, 85%). mp = 174–176 °C; 1H NMR-DMSO-d6 δ: 8.03 (d, J = 8.1 Hz, 2H), 7.86 (d, J = 8.1 Hz, 2H), 5.85 (brs, 5H), 2.67–2.66 (m, 1H), 2.51 (s, 3H), 2.38 (s, 3H), 1.67–1.09 (m, 8H), 0.86 (t, J = 8.0 Hz, 3H); anal. calc. for: $C_{19}H_{30}N_8O_2S$ (434.56): C, 52.51; H, 6.96; N, 25.79%; found: C, 52.71; H, 7.03; N, 25.59%.

4.1.3.11 2-(1-(1-(4-(N-(But-3-en-1-yl)sulfamoyl)phenyl)-5-methyl-1H-1,2,3-triazol-4-yl)ethylidene) hydrazine-1-carboximidamide ***26.*** White solid (310 mg, 89%). mp = 154–156 °C; ^{1}H NMR-DMSO-d6 δ: 8.04 (d, J = 8.1 Hz, 2H), 7.87 (d, J = 8.1 Hz, 2H), 5.79–5.68 (m, 6H), 5.01 (dd, J = 12.0 Hz, 2H), 2.92 (t, J = 8.0 Hz, 2H), 2.52 (s, 3H), 2.38 (s, 3H), 2.19–2.14 (m, 2H); ^{13}C NMR (DMSO-d_6) δ: 159.68, 145.03, 144.77, 141.76, 139.09, 135.68, 131.63, 128.46, 126.32, 124.67, 117.27, 42.62, 33.92, 14.93, 11.49; anal. calc. for $C_{16}H_{22}N_8O_2S$ (390): C, 49.22; H, 5.68; N, 28.70%; found: C, 49.42; H, 5.78; N, 28.59%.

4.1.3.12 2-(1-(1-(4-(N-Cyclopentylsulfamoyl)phenyl)-5-methyl-1H-1,2,3-triazol-4-yl)ethylidene) hydrazine-1-carboximidamide ***27.*** Buff solid (321 mg, 89%). mp = 189–190 °C; ^{1}H NMR-DMSO-d6 δ: 8.05 (d, J = 8.1 Hz, 2H), 7.86 (d, J = 8.1 Hz, 2H), 5.68 (brs, 3H), 5.56 (brs, 2H), 3.52–3.48 (m, 1H), 2.54 (s, 3H), 2.37 (s, 3H), 1.68–1.34 (m, 8H); ^{13}C NMR (DMSO-d_6) δ: 159.96, 145.22, 144.46, 142.77, 139.01, 131.42, 128.43, 126.26, 55.02, 32.95, 23.28, 14.89, 11.53; anal. calc. for: $C_{17}H_{24}N_8O_2S$ (404): C, 50.48; H, 5.98; N, 27.70%; found: C, 50.58; H, 6.07; N, 27.50%.

4.2 Biology screening

4.2.1 Antibacterial assay. The minimum inhibitory concentrations (MICs) of the tested compounds and reference antibiotics (vancomycin and gentamicin) were determined using the broth microdilution method, following Clinical and Laboratory Standards Institute (CLSI) guidelines.[60] The assay was performed at the Department of Microbiology and Immunology, Faculty of Pharmacy, Cairo University, using clinically relevant bacterial strains: methicillin-resistant *Staphylococcus aureus* (MRSA USA300) and *Acinetobacter baumannii* (AB5075). *S. aureus* cultures were grown overnight at 37 °C on tryptone soy agar, then diluted to 0.5 McFarland standard and further in cation-adjusted Mueller-Hinton broth (CAMHB) to reach ~5 × 10^5 CFU ml^{-1}. Test compounds and control antibiotics were serially diluted in 96-well plates containing bacterial suspensions. Plates were incubated aerobically at 37 °C for 18–20 hours. The MIC (μg mL^{-1}) is defined as the lowest

Open Access Article. Published on 17 June 2025. Downloaded on 11/7/2025 8:09:35 PM. This article is licensed under a Creative Commons Attribution-NonCommercial 3.0 Unported Licence.

concentration that completely inhibits visible microbial growth.[61] Data represents mean values from at least three independent experiments.

4.2.2 Time-kill kinetics assay of compounds against MRSA. MRSA USA300 cells in logarithmic growth phase were diluted to $\sim 10^6$ CFU ml^{-1} and exposed to concentrations equivalent to 4× MIC (in triplicate) of compounds **31** and **32**, and vancomycin in TSB.[29] Aliquots were collected from each treatment after 0, 2, 4, 6, 8, 10 and 24 hours of incubation at 37 °C and subsequently serially diluted in PBS. Bacteria were then transferred to TSA plates and incubated at 37 °C for 18–20 hours before viable CFU mL^{-1} was determined.

4.2.3 Anti-biofilm screening. The biofilm inhibitory potential of selected active analogs was evaluated at concentrations equivalent to their respective MICs against robust biofilm-forming strains of methicillin-resistant *Staphylococcus aureus* (MRSA, $OD_{550} = 3.655$), *Candida albicans* ($OD_{550} = 4.025$), and *Pseudomonas aeruginosa* ($OD_{550} = 3.198$). The assay was conducted at the Department of Microbiology, Faculty of Pharmacy, Al-Azhar University, Cairo. Briefly, freshly prepared seed cultures were diluted 1 : 100 and inoculated into sterile, polypropylene 96-well microtiter plates. Plates were sealed and incubated statically at 37 °C for 24 hours to allow biofilm formation. Each assay included negative control (media only) and a positive control (media with 1% inoculum). All experiments were performed in triplicate unless otherwise stated.[62]

Biofilm inhibition was quantified using the crystal violet staining method. After incubation, non-adherent cells and culture media were removed, and wells were washed three times with distilled water to eliminate planktonic cells. Adherent biofilms were stained with 125 μL of 0.1% crystal violet for 30 minutes at room temperature. Excess stain was rinsed off with distilled water, and the bound dye was solubilized in 30% acetic acid. Absorbance was measured at 550 nm.[52,63,64] The percentage of biofilm inhibition was calculated using the formula:[65]

$$\text{Biofilm inhibition (\%)} = [1 - (OD_{550} \text{ of treated wells}/OD_{550} \text{ of untreated control wells})] \times 100$$

4.2.4 MTT cytotoxicity evaluation. The MTT assay was conducted at VACSERA, Giza, Egypt, to evaluate the cytotoxic effects of the tested compounds on two normal human cell lines; HaCaT (aneuploid immortalized keratinocytes) and WI-38 (normal lung fibroblasts) as well as neuro-HiB5 cells, which are derived from embryonic (E16) Sprague-Dawley rat hippocampal tissue. Cell viability was assessed based on the colorimetric conversion of the yellow MTT reagent, reflecting mitochondrial metabolic activity.[66,67]

4.2.5 Computational analysis: likeliness, ADME and pharmacokinetics. Online platforms of ADMET (absorption, distribution, metabolism, elimination, and toxicity) profiles were used for the calculation of these properties of the most active compounds.

4.2.6 Molecular docking experiments. Two molecular targets from methicillin-resistant *Staphylococcus aureus*; G-acyl penicillin-binding protein 2a (PBP2a, PDB ID: 1MWT) and dihydropteroate synthase (DHPS, PDB ID: 6CLV) were selected for molecular docking studies. Compounds **23** and **24** were docked into the active sites of both enzymes.[68] To validate the docking protocol, re-docking simulations were first performed using the crystal structures. Enzyme structures were prepared using AutoDock Tools,[69] while docking simulations were carried out *via* PyRx.[70] Visualization and analysis of docking results were completed using Discovery Studio Visualizer.[71] Input files were generated using AutoDock Tools, and the docking grid was set to 90 × 90 × 90 points with a spacing of 0.375 Å, encompassing nearly the entire protein surface.

Ligands were constructed using AutoDock's ligand builder, with geometry optimization performed using the CHARMm force field.[72] Docking calculations were prepared using Python scripts from the AutoDock suite. Each ligand underwent 50 docking runs, and the resulting poses were clustered using a 1.8 Å RMSD cutoff. The conformational search utilized the Lamarckian Genetic Algorithm,[51,73–76] with a starting population of 150 individuals and up to 25 000 000 energy evaluations. The most populated low-energy clusters were selected for further analysis.

Molecular dynamics (MD) simulations were subsequently carried out to assess the stability of compound 23 in complex with the target proteins, compared to reference drugs. Desmond version 3.8, utilizing the OPLS2005 force field[77] and developed by D. E. Shaw Research, was used for the simulations. Production MD was performed under isothermal-isobaric (NPT) conditions at 300 K and 1 bar using Langevin dynamics, over three independent 100 ns simulation runs.

Data availability

The data supporting this article have been included in the main manuscript and ESI.†

Author contributions

I confirm that the contribution of each author is outlined in the manuscript below, with some authors contributing to multiple roles. I am responsible for ensuring the accuracy of these descriptions, which have been agreed upon by all authors involved. A. H. and M. M. E.: synthesis and refinement of methodology, spectroscopic analysis, and drafting the original manuscript. A. N. H., H. G. E., and A. S. M.: conceptualization, supervision, manuscript writing and review, and project administration. All authors have read and approved the final version of the manuscript. H. T. N. E. and Y. N.: antimicrobial screening, methodology development, and drafting the original manuscript. M. A.: molecular modeling, biochemical data evaluation and discussion, manuscript writing, review and editing, and funding acquisition. A. M., K. S., and D. G. T. P.: biological evaluation of target compounds, molecular modeling, data analysis, and partial funding acquisition. M. M. E. and A. S. M.: proposal writing, supervision, and synthesis.

 © 2025 The Author(s). Published by the Royal Society of Chemistry

Open Access Article. Published on 17 June 2025. Downloaded on 11/7/2025 8:09:35 PM. This article is licensed under a Creative Commons Attribution-NonCommercial 3.0 Unported Licence.

Conflicts of interest

The authors declare that they have no known competing financial interests or personal relationships that could have appeared to influence the work reported in this paper.

Acknowledgements

This work was funded by the Deanship of Graduate Studies and Scientific Research at Jouf University under grant no. (DGSSR-2024-01-01038) and supported by grant number C21-113 from the Science, Technology & Innovation Funding Authority (STDF).

References

1 M. Dulon, F. Haamann, C. Peters, A. Schablon and A. Nienhaus, MRSA prevalence in European healthcare settings: a review, *BMC Infect. Dis.*, 2011, **11**, 1–13.
2 J. M. Blair, M. A. Webber, A. J. Baylay, D. O. Ogbolu and L. J. Piddock, Molecular mechanisms of antibiotic resistance, *Nat. Rev. Microbiol.*, 2015, **13**(1), 42–51.
3 M. Terreni, M. Taccani and M. Pregnolato, New antibiotics for multidrug-resistant bacterial strains: latest research developments and future perspectives, *Molecules*, 2021, **26**(9), 2671.
4 S. Boyle-Vavra, S. Yin, M. Challapalli and R. S. Daum, Transcriptional induction of the penicillin-binding protein 2 gene in Staphylococcus aureus by cell wall-active antibiotics oxacillin and vancomycin, *Antimicrob. Agents Chemother.*, 2003, **47**(3), 1028–1036.
5 M. M. Elsebaei, H. G. Ezzat, A. M. Helal, M. H. El-Shershaby, M. S. Abdulrahman, M. Alsedawy, *et al.*, Rational design and synthesis of novel phenyltriazole derivatives targeting MRSA cell wall biosynthesis, *RSC Adv.*, 2024, **14**(54), 39977–39994.
6 W. S. Champney and R. Burdine, Macrolide antibiotics inhibit 50S ribosomal subunit assembly in Bacillus subtilis and Staphylococcus aureus, *Antimicrob. Agents Chemother.*, 1995, **39**(9), 2141–2144.
7 M. Almaghrabi, A. Musa, A. K. B. Aljohani, H. E. A. Ahmed, M. Alsulaimany, S. F. Miski, *et al.*, Introducing of novel class of pyrano[2,3-c]pyrazole-5-carbonitrile analogs with potent antimicrobial activity, DNA gyrase inhibition, and prominent pharmacokinetic and CNS toxicity profiles supported by molecular dynamic simulation, *J. Biomol. Struct. Dyn.*, 2024, **42**(18), 9529–9546.
8 A. M. Fouda, A. H. Hassan, E. M. Eliwa, H. E. A. Ahmed, A.-A. M. Al-Dies, A. M. Omar, *et al.*, Targeted potent antimicrobial benzochromene-based analogues: Synthesis, computational studies, and inhibitory effect against 14α-Demethylase and DNA Gyrase, *Bioorg. Chem.*, 2020, **105**, 104387.
9 M. M. Elsebaei, H. Mohammad, M. Abouf, N. S. Abutaleb, Y. A. Hegazy, A. Ghiaty, *et al.*, Alkynyl-containing phenylthiazoles: Systemically active antibacterial agents effective against methicillin-resistant Staphylococcus aureus (MRSA), *Eur. J. Med. Chem.*, 2018, **148**, 195–209.
10 S. M. Swaney, H. Aoki, M. C. Ganoza and D. L. Shinabarger, The oxazolidinone linezolid inhibits initiation of protein synthesis in bacteria, *Antimicrob. Agents Chemother.*, 1998, **42**(12), 3251–3255.
11 S. A. Grim, R. P. Rapp, C. A. Martin and M. E. Evans, Trimethoprim-sulfamethoxazole as a viable treatment option for infections caused by methicillin-resistant Staphylococcus aureus, *Pharmacotherapy*, 2005, **25**(2), 253–264.
12 C. Rayner and W. J. Munckhof, Antibiotics currently used in the treatment of infections caused by Staphylococcus aureus, *Intern. Med. J.*, 2005, **35**(Suppl 2), S3–S16.
13 H. E. A. Ahmed, S. K. Ihmaid, A. M. Omar, A. M. Shehata, H. S. Rateb, M. F. Zayed, *et al.*, Design, synthesis, molecular docking of new lipophilic acetamide derivatives affording potential anticancer and antimicrobial agents, *Bioorg. Chem.*, 2018, **76**, 332–342.
14 A. A. Abuelkhir, Y. I. Nagy, T. Gamal, A. M. Abdelhalim, A. S. Attia, A. S. Mayhoub, *et al.*, Small Molecule Alkynyl-Phenylaminoguanidines: A New Weapon Against Multi-Drug Resistant Bacteria, *ChemistrySelect*, 2025, **10**(4), e202404320.
15 Organization WH, *2019 Antibacterial Agents in Clinical Development: an Analysis of the Antibacterial Clinical Development Pipeline*, 2019.
16 R. A. Fisher, B. Gollan and S. Helaine, Persistent bacterial infections and persister cells, *Nat. Rev. Microbiol.*, 2017, **15**(8), 453–464.
17 E. Pontali, M. C. Raviglione and G. B. Migliori, Regimens to treat multidrug-resistant tuberculosis: past, present and future perspectives, *Eur. Respir. Rev.*, 2019, **28**(152), 190035.
18 K. Iwamoto, M. Moriwaki, R. Miyake and M. Hide, Staphylococcus aureus in atopic dermatitis: Strain-specific cell wall proteins and skin immunity, *Allergol. Int.*, 2019, **68**(3), 309–315.
19 R. M. Hassan, M. G. Elanany, M. M. Mostafa, R. H. A. Yousef and S. T. Salem, Whole genome characterization of methicillin resistant Staphylococcus aureus in an Egyptian Tertiary Care Hospital, *J. Microbiol. Immunol. Infect.*, 2023, 802–814.
20 R. Pavillard, K. Harvey, D. Douglas, A. Hewstone, J. Andrew, B. Collopy, *et al.*, Epidemie of hospital-acquired infection due to methicillin-resistant Staphylococcus aureus in major Victorian hospitals, *Med. J. Aust.*, 1982, **1**(11), 451–454.
21 J. M. Kwiecinski and A. R. Horswill, Staphylococcus aureus bloodstream infections: pathogenesis and regulatory mechanisms, *Curr. Opin. Microbiol.*, 2020, **53**, 51–60.
22 T. Foster, 39 - Staphylococcus aureus, *Mol. Med. Microbiol.*, 2002, **2**, 839–888.
23 H. Nikaido, Prevention of drug access to bacterial targets: permeability barriers and active efflux, *Science*, 1994, **264**(5157), 382–388.
24 E. Yamashita, M. V. Zhalnina, S. D. Zakharov, O. Sharma and W. A. Cramer, Crystal structures of the OmpF porin: function in a colicin translocon, *EMBO J.*, 2008, **27**(15), 2171–2180.
25 R. O'Shea and H. E. Moser, Physicochemical properties of antibacterial compounds: implications for drug discovery, *J. Med. Chem.*, 2008, **51**(10), 2871–2878.

Open Access Article. Published on 17 June 2025. Downloaded on 11/7/2025 8:09:35 PM.
This article is licensed under a Creative Commons Attribution-NonCommercial 3.0 Unported Licence.

26 C. Zhao, K. Rakesh, L. Ravidar, W.-Y. Fang and H.-L. Qin, Pharmaceutical and medicinal significance of sulfur (SVI)-Containing motifs for drug discovery: A critical review, *Eur. J. Med. Chem.*, 2019, **162**, 679–734.

27 S. S. Atwa, M. Hagras, A. S. Mayhoub and M. Elsebaei, Synthesis Of Some New Azole Derivatives As Antibacterial Agents, *Al-Azhar J. Pharm. Sci.*, 2024, **69**(1), 108–129.

28 I. Eid, M. M. Elsebaei, H. Mohammad, M. Hagras, C. E. Peters, Y. A. Hegazy, *et al.*, Arylthiazole antibiotics targeting intracellular methicillin-resistant Staphylococcus aureus (MRSA) that interfere with bacterial cell wall synthesis, *Eur. J. Med. Chem.*, 2017, **139**, 665–673.

29 M. M. Elsebaei, H. Mohammad, M. Abouf, N. S. Abutaleb, Y. A. Hegazy, A. Ghiaty, *et al.*, Alkynyl-containing phenylthiazoles: Systemically active antibacterial agents effective against methicillin-resistant Staphylococcus aureus (MRSA), *Eur. J. Med. Chem.*, 2018, **148**, 195–209.

30 H. Mohammad, A. S. Mayhoub, M. Cushman and M. N. Seleem, Anti-biofilm activity and synergism of novel thiazole compounds with glycopeptide antibiotics against multidrug-resistant staphylococci, *J. Antibiotics*, 2015, **68**(4), 259–266.

31 H. Mohammad, P. V. Reddy, D. Monteleone, A. S. Mayhoub, M. Cushman and M. N. Seleem, Synthesis and antibacterial evaluation of a novel series of synthetic phenylthiazole compounds against methicillin-resistant Staphylococcus aureus (MRSA), *Eur. J. Med. Chem.*, 2015, **94**, 306–316.

32 H. Mohammad, W. Younis, L. Chen, C. E. Peters, J. Pogliano, K. Pogliano, *et al.*, Phenylthiazole Antibacterial Agents Targeting Cell Wall Synthesis Exhibit Potent Activity in Vitro and in Vivo against Vancomycin-Resistant Enterococci, *J. Med. Chem.*, 2017, **60**(6), 2425–2438.

33 M. Hagras, N. S. Abutaleb, A. O. Ali, J. A. Abdel-Aleem, M. M. Elsebaei, M. N. Seleem, *et al.*, Naphthylthiazoles: Targeting Multidrug-Resistant and Intracellular Staphylococcus aureus with Biofilm Disruption Activity, *ACS Infect. Dis.*, 2018, **4**(12), 1679–1691.

34 A. M. Sayed, N. S. Abutaleb, A. Kotb, H. G. Ezzat, M. N. Seleem, A. S. Mayhoub, *et al.*, Arylpyrazole as selective anti-enterococci; synthesis and biological evaluation of novel derivatives for their antimicrobial efficacy, *J. Heterocycl. Chem.*, 2023, **60**(1), 134–144.

35 I. G. Shahin, K. O. Mohamed, A. T. Taher, M. M. Elsebaei, A. S. Mayhoub, A. E. Kassab, *et al.*, New Phenylthiazoles: Design, Synthesis, and Biological Evaluation as Antibacterial, Antifungal, and Anti-COVID-19 Candidates, *Chem. Biodiversity*, 2023, e202301143.

36 M. Omara, M. Hagras, M. M. Elsebaie, N. S. Abutaleb, H. T. N. El-Din, M. O. Mekhail, *et al.*, Exploring novel aryl/heteroaryl-isosteres of phenylthiazole against multidrug-resistant bacteria, *RSC Adv.*, 2023, **13**(29), 19695–19709.

37 A. Mancy, N. S. Abutaleb, M. M. Elsebaei, A. Y. Saad, A. Kotb, A. O. Ali, *et al.*, Balancing physicochemical properties of phenylthiazole compounds with antibacterial potency by modifying the lipophilic side chain, *ACS Infect. Dis.*, 2019, **6**(1), 80–90.

38 M. M. Elsebaei, H. Mohammad, A. Samir, N. S. Abutaleb, A. B. Norvil, A. R. Michie, *et al.*, Lipophilic efficient phenylthiazoles with potent undecaprenyl pyrophosphatase inhibitory activity, *Eur. J. Med. Chem.*, 2019, **175**, 49–62.

39 H. T. N. El-Din, M. M. Elsebaie, N. S. Abutaleb, A. M. Kotb, A. S. Attia, M. N. Seleem, *et al.*, Expanding the structure–activity relationships of alkynyl diphenylurea scaffold as promising antibacterial agents, *RSC Med. Chem.*, 2023, **14**(2), 367–377.

40 Y. Hosny, N. S. Abutaleb, M. Omara, M. Alhashimi, M. M. Elsebaei, H. S. Elzahabi, *et al.*, Modifying the lipophilic part of phenylthiazole antibiotics to control their drug-likeness, *Eur. J. Med. Chem.*, 2020, **185**, 111830.

41 I. G. Shahin, K. O. Mohamed, A. T. Taher, M. M. Elsebaei, A. S. Mayhoub, A. E. Kassab, *et al.*, New Phenylthiazoles: Design, Synthesis, and Biological Evaluation as Antibacterial, Antifungal, and Anti-COVID-19 Candidates, *Chem. Biodiversity*, 2023, **20**(11), e202301143.

42 A. Mancy, Synthesis And Evaluation Of Antimicrobial Activity Of Arylazole Derivatives, *Al-Azhar J. Pharm. Sci.*, 2019, **60**(2), 43–50.

43 A. Hammad, N. S. Abutaleb, M. M. Elsebaei, A. B. Norvil, M. Alswah, A. O. Ali, *et al.*, From phenylthiazoles to phenylpyrazoles: broadening the antibacterial spectrum toward carbapenem-resistant bacteria, *J. Med. Chem.*, 2019, **62**(17), 7998–8010.

44 M. M. Elsebaei, N. S. Abutaleb, A. A. Mahgoub, D. Li, M. Hagras, H. Mohammad, *et al.*, Phenylthiazoles with nitrogenous side chain: An approach to overcome molecular obesity, *Eur. J. Med. Chem.*, 2019, **182**, 111593.

45 M. M. Elsebaie, H. T. N. El-Din, N. S. Abutaleb, A. A. Abuelkhir, H.-W. Liang, A. S. Attia, *et al.*, Exploring the structure-activity relationships of diphenylurea as an antibacterial scaffold active against methicillin-and vancomycin-resistant Staphylococcus aureus, *Eur. J. Med. Chem.*, 2022, **234**, 114204.

46 M. Alswah, Synthesis And Biological Evaluation Of Novel Pyrazolo [3, 4-D] Pyrimidine Derivatives Of Expected Anticancer Activity, *Al-Azhar J. Pharm. Sci.*, 2021, **64**(2), 80–92.

47 A. M. Helal, A. M. Sayed, M. Omara, M. M. Elsebaei and A. S. Mayhoub, Peptidoglycan pathways: there are still more, *RSC Adv.*, 2019, **9**(48), 28171–28185.

48 K. El-Gamal, F. Sherbiny, A. El-Morsi, H. Abu-El-khair, I. Eissa and M. El-Sebaei, Design, synthesis and antimicrobial evaluation of some novel quinoline derivatives, *Pharm. Pharmacol. Int. J.*, 2015, **2**(5), 165–177.

49 S. A. Grim, R. P. Rapp, C. A. Martin and M. E. Evans, Trimethoprim-sulfamethoxazole as a viable treatment option for infections caused by methicillin-resistant Staphylococcus aureus, *Pharmacotherapy*, 2005, **25**(2), 253–264.

50 T. A. Łeski and A. Tomasz, Role of penicillin-binding protein 2 (PBP2) in the antibiotic susceptibility and cell wall cross-linking of Staphylococcus aureus: evidence for the

 © 2025 The Author(s). Published by the Royal Society of Chemistry

Open Access Article. Published on 17 June 2025. Downloaded on 11/7/2025 8:09:35 PM. This article is licensed under a Creative Commons Attribution-NonCommercial 3.0 Unported Licence.

cooperative functioning of PBP2, PBP4, and PBP2A, *J. Bacteriol.*, 2005, **187**(5), 1815–1824.

51 M. Almaghrabi, A. Musa, A. K. B. Aljohani, H. E. A. Ahmed, M. Alsulaimany, S. F. Miski, *et al.*, Introducing of novel class of pyrano[2,3-c]pyrazole-5-carbonitrile analogs with potent antimicrobial activity, DNA gyrase inhibition, and prominent pharmacokinetic and CNS toxicity profiles supported by molecular dynamic simulation, *J. Biomol. Struct. Dyn.*, 2023, 1–18.

52 A. M. Omar, S. Ihmaid, E. E. Habib, S. S. Althagfan, S. Ahmed, H. S. Abulkhair, *et al.*, The rational design, synthesis, and antimicrobial investigation of 2-Amino-4-Methylthiazole analogues inhibitors of GlcN-6-P synthase, *Bioorg. Chem.*, 2020, **99**, 103781.

53 N. Lv, Q. Kong, H. Zhang and J. Li, Discovery of novel Staphylococcus aureus penicillin binding protein 2a inhibitors by multistep virtual screening and biological evaluation, *Bioorg. Med. Chem. Lett*, 2021, **41**, 128001.

54 H. Lade and J.-S. Kim, Bacterial Targets of Antibiotics in Methicillin-Resistant Staphylococcus aureus, *Antibiotics*, 2021, **10**(4), 398.

55 N. H. Amin, M. T. El-Saadi, A. A. Ibrahim and H. M. Abdel-Rahman, Design, synthesis and mechanistic study of new 1,2,4-triazole derivatives as antimicrobial agents, *Bioorg. Chem.*, 2021, **111**, 104841.

56 C. Y. Jia, J. Y. Li, G. F. Hao and G. F. Yang, A drug-likeness toolbox facilitates ADMET study in drug discovery, *Drug Discov. Today*, 2020, **25**(1), 248–258.

57 D. H. O'Donovan, C. De Fusco, L. Kuhnke and A. Reichel, Trends in molecular properties, bioavailability, and permeability across the bayer compound collection: miniperspective, *J. Med. Chem.*, 2023, **66**(4), 2347–2360.

58 P. Banerjee, A. O. Eckert, A. K. Schrey and R. Preissner, ProTox-II: a webserver for the prediction of toxicity of chemicals, *Nucleic Acids Res.*, 2018, **46**(W1), W257–W63.

59 A. Angeli, A. Petrou, V. Kartsev, B. Lichitsky, A. Komogortsev, C. Capasso, *et al.*, Synthesis, Biological and In Silico Studies of Griseofulvin and Usnic Acid Sulfonamide Derivatives as Fungal, Bacterial and Human Carbonic Anhydrase Inhibitors, *Int. J. Mol. Sci.*, 2023, **24**(3), 2802.

60 J. An, G. Y. Zuo, X. Y. Hao, G. C. Wang and Z. S. Li, Antibacterial and synergy of a flavanonol rhamnoside with antibiotics against clinical isolates of methicillin-resistant Staphylococcus aureus (MRSA), *Phytomedicine*, 2011, **18**(11), 990–993.

61 N. Rezki, S. A. Al-Sodies, H. E. A. Ahmed, S. Ihmaid, M. Messali, S. Ahmed, *et al.*, A novel dicationic ionic liquids encompassing pyridinium hydrazone-phenoxy conjugates as antimicrobial agents targeting diverse high resistant microbial strains, *J. Mol. Liq.*, 2019, **284**, 431–444.

62 G. A. O'Toole, Microtiter dish biofilm formation assay, *J. Vis. Exp.*, 2011, (47), 2437.

63 K. Alam, D. A. A. Farraj, E. F. S. Mah, M. A. Yameen, M. S. Elshikh, R. M. Alkufeidy, *et al.*, Anti-biofilm activity of plant derived extracts against infectious pathogen-Pseudomonas aeruginosa PAO1, *J. Infect. Public Health.*, 2020, **13**(11), 1734–1741.

64 H. E. A. Ahmed, H. A. Abdel-Salam and M. A. Shaker, Synthesis, characterization, molecular modeling, and potential antimicrobial and anticancer activities of novel 2-aminoisoindoline-1, 3-dione derivatives, *Bioorg. Chem.*, 2016, **66**, 1–11.

65 A. Hend and Y. A. F. El-sayed, Correlation between biofilm formation and multidrug resistance in clinical isolates of Pseudomonas aeruginosa, *Microbes Infect. Dis.*, 2021, **2**(3), 541–549.

66 T. Mosmann, Rapid colorimetric assay for cellular growth and survival: application to proliferation and cytotoxicity assays, *J. Immunol. Methods*, 1983, **65**(1–2), 55–63.

67 F. Demirci and K. H. C. Başer, *Bioassay Techniques for Drug Development*, ed. Atta-ur-Rahman, M. Iqbal Choudhary and William J. Thomsen, Harwood Academic Publishers, Amsterdam, The Netherlands, 2001, xii + 223 pp. 15.5 × 23.5 cm. $79.00, ISBN 90-5823-051-1.*J. Nat. Prod.*, 2002, 65(7):1086–.

68 S. Howard, V. Berdini, J. A. Boulstridge, M. G. Carr, D. M. Cross, J. Curry, *et al.*, Fragment-Based Discovery of the Pyrazol-4-yl Urea (AT9283), a Multitargeted Kinase Inhibitor with Potent Aurora Kinase Activity, *J. Med. Chem.*, 2009, **52**(2), 379–388.

69 G. M. Morris, D. S. Goodsell, R. S. Halliday, R. Huey, W. E. Hart, R. K. Belew, *et al.*, Automated docking using a Lamarckian genetic algorithm and an empirical binding free energy function, *J. Comput. Chem.*, 1998, **19**(14), 1639–1662.

70 S. Dallakyan and A. J. Olson, Small-molecule library screening by docking with PyRx, *Methods Mol. Biol.*, 2015, **1263**, 243–250.

71 M. A. Soliman, H. E. Ahmed, E. H. Eltamany, A. T. Boraei, A. Aljuhani, S. A. Salama, R. Alghamdi, A. K. Aljohani, M. Almaghrabi and M. R. Aouad, Novel bis-benzimidazole-triazole hybrids: anticancer study, in silico approaches, and mechanistic investigation, *Future Med. Chem.*, 2025, **17**(1), 93–107.

72 K. Vanommeslaeghe, E. Hatcher, C. Acharya, S. Kundu, S. Zhong, J. Shim, *et al.*, CHARMM general force field: A force field for drug-like molecules compatible with the CHARMM all-atom additive biological force fields, *J. Comput. Chem.*, 2010, **31**(4), 671–690.

73 A. A. Awaji, W. A. Z. E. Zaloa, M. A. Seleem, M. Alswah, M. M. Elsebaei, A. H. Bayoumi, *et al.*, N- and s-substituted Pyrazolopyrimidines: A promising new class of potent c-Src kinase inhibitors with prominent antitumor activity, *Bioorg. Chem.*, 2024, **145**, 107228.

74 A. M. Malebari, H. E. A. Ahmed, S. K. Ihmaid, A. M. Omar, Y. A. Muhammad, S. S. Althagfan, *et al.*, Exploring the dual effect of novel 1,4-diarylpyranopyrazoles as antiviral and anti-inflammatory for the management of SARS-CoV-2 and associated inflammatory symptoms, *Bioorg. Chem.*, 2023, **130**, 106255.

75 M. T. Khayat, H. E. A. Ahmed, A. M. Omar, Y. A. Muhammad, K. A. Mohammad, A. M. Malebari, *et al.*, A novel class of phenylpyrazolone-sulphonamides rigid synthetic

Open Access Article. Published on 17 June 2025. Downloaded on 11/7/2025 8:09:35 PM.
This article is licensed under a Creative Commons Attribution-NonCommercial 3.0 Unported Licence.

anticancer molecules selectively inhibit the isoform IX of carbonic anhydrases guided by molecular docking and orbital analyses, *J. Biomol. Struct. Dyn.*, 2023, 1–19.

76 M. Alsehli, A. Aljuhani, S. K. Ihmaid, S. M. El-Messery, D. I. A. Othman, A.-A. A. A. El-Sayed, *et al.*, Design and Synthesis of Benzene Homologues Tethered with 1,2,4-Triazole and 1,3,4-Thiadiazole Motifs Revealing Dual MCF-7/HepG2 Cytotoxic Activity with Prominent Selectivity via Histone Demethylase LSD1 Inhibitory Effect, *Int. J. Mol. Sci.*, 2022, **23**(15), 8796.

77 D. E. Shaw, P. Maragakis, K. Lindorff-Larsen, S. Piana, R. O. Dror, M. P. Eastwood, *et al.*, Atomic-level characterization of the structural dynamics of proteins, *Science*, 2010, **330**(6002), 341–346.

 © 2025 The Author(s). Published by the Royal Society of Chemistry